A 187Re-187Os, 87Rb-86Sr, highly siderophile and incompatible trace element study of some carbonaceous, ordinary and enstatite chondrite meteorites

Nicole Phelan, James M. D. Day, Jasmeet K. Dhaliwal, Yang Liu, Christopher A. Corder, Caleb Strom, Emily Pringle, Nelly Assayag, Pierre Cartigny, Kurt Marti, et al.

Available online at www.sciencedirect.com

ScienceDirect

Geochimica et Cosmochimica Acta 318 (2022) 19–54

Geochimica et Cosmochimica Acta

www.elsevier.com/locate/gca

A ^{187}Re-^{187}Os, ^{87}Rb-^{87}Sr, highly siderophile and incompatible trace element study of some carbonaceous, ordinary and enstatite chondrite meteorites

Nicole Phelan [a,*], James M.D. Day [a], Jasmeet K. Dhaliwal [a], Yang Liu [b], Christopher A. Corder [a], Caleb Strom [a], Emily Pringle [a], Nelly Assayag [c], Pierre Cartigny [c], Kurt Marti [a], Frédéric Moynier [d]

[a] *Scripps Institution of Oceanography, University of California San Diego, La Jolla, CA 92093-0244, USA*
[b] *Jet Propulsion Laboratory, M/S 183-301, 4800 Oak Grove Drive, Pasadena, CA 91109, USA*
[c] *Université de Paris, Institut de physique du globe de Paris, CNRS, F-75005 Paris, France*
[d] *Institut de Physique du Globe de Paris, Sorbonne Paris Cité, Univ. Paris Diderot, UMR 7154 CNRS, 1 rue Jussieu, 75238 Paris, France*

Received 14 June 2021; accepted in revised form 14 November 2021; available online 19 November 2021

Abstract

New ^{187}Re-^{187}Os, ^{87}Rb-^{87}Sr, triple O-isotope isotope, bulk rock highly siderophile- (HSE: Os, Ir, Ru, Pt, Pd, Re), major- and trace-element abundance data are reported for a variety of carbonaceous, ordinary and enstatite chondrite meteorites. In addition, new mineral chemical data are reported for the Chelyabinsk LL5 ordinary chondrite fall for comparison with existing chondrite data and to investigate element sequestration into metal and mineral phases within some chondrites. The focus of the study is to link the variations observed in the HSE abundances and Re-Os isotopes with other isotopic and elemental data to explore the relative roles of sample sizes, terrestrial alteration and parent body processes more fully on chondrite meteorite compositions. Trace element variations in Chelyabinsk silicate, oxide and metal grains highlight the importance of geochemical heterogeneity imparted by mineralogical variations and mode effects, as well as sample size. Using a range of sample powder aliquot sizes, it is possible to show that this becomes significant for the HSE at <0.1 g. Variations in high field strength elements relative abundances (HFSE: Ti, Zr, Nb, Ta, Hf) are also identified within individual aliquots of carbonaceous chondrite Ivuna, emphasizing the importance of complete dissolution of refractory phases. The range of fall and find meteorites examined here demonstrates that terrestrial alteration effects revealed for trace elements (e.g., Ba, U, Sr) do not correlate particularly well with Re/Os variations. Instead, the Re/Os ratios of carbonaceous chondrites are susceptible to disturbance, more so than indicated by incompatible trace element systematics, with the Murchison CM2 carbonaceous chondrite showing significant Re/Os fractionation between sample aliquots. For sample aliquots measured that do not show significant mode or terrestrial alteration effects, parent body processes appear to be largely restricted to thermal metamorphism and dehydration. Including data for this study, the combined published dataset for Re-Os isotope and HSE abundances now extends to 33 ordinary, 39 carbonaceous, 27 enstatite and 6 Rumuruti chondrites. The range in absolute HSE abundances among these meteorite groups is ~30%, with all chondrites having, within uncertainties, the same average Os, Ir, Ru, Pt and Pd abundances. Notably, carbonaceous chondrites have long-term Re/Os ~ 8% lower than for the other chondrite groups. If chondrite groups are representative of early planetary feedstocks, then the measured ^{187}Os/^{188}Os of ordinary chondrites make them a close match to the composition of the bulk silicate Earth. Assuming ~0.5% late accretion of ordinary chondrites to Earth, this

* Corresponding author.
E-mail address: ndphelan@ucsd.edu (N. Phelan).

https://doi.org/10.1016/j.gca.2021.11.020

would result in a long-term Rb/Sr ratio ~0.6% higher than from late accretion of carbonaceous chondrites, indicating that ordinary chondrites are a potentially attractive source for moderately volatile enrichment.

Keywords: Carbonaceous; Ordinary; Enstatite; Chondrites; Highly siderophile elements; Incompatible trace elements; Strontium isotopes; Osmium isotopes

1. INTRODUCTION

Meteorites offer unique insights into the chronology of our Solar System, as well as a fundamental understanding as to how planetary bodies formed and evolved (e.g., Anders, 1971; Lauretta and McSween, 2006; Day, 2015). The study of chondrite meteorites has provided the foundations for understanding the constituent materials supplied to the Solar System, as well as the building blocks for planet formation (e.g., Anders and Grevesse, 1989; McDonough and Sun, 1995; Righter and Drake, 1997; Warren, 2011; Heck et al., 2020). In particular, studies of the highly siderophile elements (HSE: Os, Ir, Ru, Rh, Pt, Pd, Re, Au) and Os isotopic variations in chondrites carry information on the materials involved in the formation of the Solar System (e.g., Brandon et al., 2005a,b; Yokoyama and Walker, 2016), condensation processes inherent in the early solar nebula (Palme and Wlotzka, 1976), and the bulk compositional variations in chondrites and their components (e.g., Walker et al., 2002; Horan et al., 2003; Fischer-Gödde et al., 2010; Archer et al., 2014). Some of these studies have also demonstrated the susceptibility of the HSE and Re-Os isotope system to parent body processes, complicating interpretation of this data in certain instances. While focused analysis of geochemical compositions allows in-depth understanding of individual chemical attributes, combined isotope and elemental studies (mineral chemistry, strontium isotopes, trace- and major-element abundances etc.) in individual sample aliquots hold promise for distinguishing processes and event timings that modify compositions in chondrites.

Another critical issue in chondrite meteorite studies is appropriate sample size to address small-scale features and individual components versus bulk compositions. While smaller sample sizes can give indications of heterogeneities within chondrites (e.g., Kadlag and Becker, 2015; Kadlag and Becker, 2017), enabling assessment of nucleosynthetic components and constituent mineral phases (e.g., Palme and Wlotzka, 1976; Daly et al., 2017), bulk samples are likely to be more helpful for understanding parental asteroid and reservoir characteristics. Both sample types are therefore useful for understanding chondrites and their components, with prior studies of the HSE and Re-Os isotopes in chondrites revealing important heterogeneities in chondrite components (Walker et al., 2002; Horan et al., 2003; Fischer-Gödde et al., 2010). Untangling the effects of sample size and representativeness, in conjunction with a fuller understanding of chemical components and isotope systems in chondrites, remain important areas of investigation for a fuller understanding of chondrite parent body processes.

Motivated by the need for further work on chondrite components (c.f., Fremlindge, Calcium-Aluminum Inclusions (CAI's), chondrules, matrix materials) and on chondrite meteorite falls and finds (Day, 2016), this study explores a combined ^{87}Rb-^{87}Sr, ^{187}Re-^{187}Os, O-isotope, major-, trace- and HSE abundance approach to individual aliquots of chondrite meteorites. In some instances, this is partly forced by available sample sizes, but also enables us to address the issue of representative sample size. This is particularly important for existing and future missions to asteroidal bodies with compositions similar to chondrites. Our examination is also valuable for assessing what can be learned from approaching different scales of investigation within chondrites. The goals of the work are two-fold. In the first instance, it aims to expand available HSE and Re-Os isotope data to a wider range of chondrite compositions than hitherto examined. As part of this goal, the first Re-Os isotope and HSE abundance data for the Chelyabinsk ordinary chondrite fall are presented, along with new data for a range of carbonaceous, ordinary and enstatite falls and finds. In addition to the new data for Chelyabinsk, a detailed description of the samples analyzed in this study and the mineralogical compositions are also presented. The second goal is to examine the relative roles of terrestrial alteration, mode-effects, and parent body processes, particularly regarding the HSE distribution within and among the chondrite classes.

2. SAMPLES

A range of compositional and metamorphic types of carbonaceous, ordinary and enstatite chondrites were analyzed to understand, more fully, the geochemical variations in these meteorites. Non-analytical characteristics of examined samples, including distinction between falls and finds, are given in Table 1. Falls refer to samples collected immediately or soon after the meteorite was seen falling to Earth, whereas finds refer to samples that have spent an unknown amount of time in the terrestrial surface environment prior to collection. Carbonaceous chondrites analyzed in this study consist of two CI, one CB, one CK, five CM, three CV and two C2-ungrouped chondrites. These analyses increase the number of individual carbonaceous chondrite meteorites analyzed for HSE abundances and Os isotopes to 39, spanning CI1, CR2, CM2, CO3, CV3, CK3-4, CB and C2 types (see Walker et al., 2002; Horan et al., 2003; Fischer-Gödde et al., 2010; van Acken et al., 2011; Archer et al., 2014; Goderis et al., 2017). The ordinary chondrites in this study include four H, eight L and two LL chondrites. These analyses increase the total number of ordinary chondrites measured for HSE abundances

Table 1
Non-analytical characteristics of chondrite meteorites analyzed in this study.

Chondrite	Sample ID	Classification	Fall/ Find	Mass of original chondrite	Mass powdered (g)	Year	Fall Area
Carbonaceous							
NWA 5958		$C2_{ung}$	Find	286 g	0.030	2009	Morocco
Tagish Lake	MS 2292C	$C2_{ung}$	Fall	10 kg	0.191	2000	British Columbia, Canada
Gujba		CBa	Fall	100 kg	0.024	1984	Yobe, Nigeria
Ivuna		CI1	Fall	705 g	0.002	1938	Mbeya, Tanzania
Orgueil		CI1	Fall	14 kg	0.007	1864	Midi-Pyrenees, France
Maralinga		$CK4_{an}$	Find	3.39 kg	0.100	1974	South Australia
Banten		CM2	Fall	629 g	0.157	1933	Jawa Barat, Indonesia
Cold Bokkeveld		CM2	Fall	5.3 kg	0.009	1838	Western Cape, South Africa
Murchison	Main SIGL	CM2	Fall	100 kg	0.119	1969	Victoria, Australia
	MTF 2005	CM2			0.101		
Murray		CM2	Fall	12.6 kg	0.126	1950	Kentucky, USA
Allende	USNM 3529	CV3	Fall	2 t	0.586	1969	Chihuahua, Mexico
GRA 06101		CV3	Find	3.56 kg	0.022	2006	Antarctica
Vigarano		CV3	Fall	15 kg		1910	Emilia-Romagna, Italy
NWA 4502		CV3	Find	100 kg	0.030	2005	Algeria
Ordinary							
Fayetteville		H4	Fall	2.36 kg	0.159	1934	Arkansas, USA
Forest City	AMNH 2421	H5	Fall	152 kg	0.096	1890	Iowa, USA
Pultusk		H5	Fall	250 kg	0.094	1868	Ostroleka, Poland
Richardton		H5	Fall	90 kg	0.055	1918	North Dakota, USA
NWA 869		L3-6	Find	2 t	0.098	2000	Northwest Africa
Khohar		L3.6	Fall	9.7 kg	0.015	1910	Madhya Pradesh, India
Saratov		L4	Fall	200 kg	0.125	1918	Saratovkaya, Russia
Aïr		L6	Fall	24 kg	0.146	1925	Agadez, Niger
Kunashak	Lg Slice	L6	Fall	200 kg	0.200	1949	Chelyabinskaya, Russia
	LAT	L6					
Kyle		L6	Find	7.78 kg	0.171	1965	Texas, USA
Peace River	MTF 2116, Main Mass	L6	Fall	45.76 kg	0.097	1963	Alberta, Canada
Chelyabinsk		LL5	Fall	1 t	0.208	2013	Chelyabinskaya, Russia
Olivenza		LL5	Fall	150 kg	0.005	1924	Extremadura, Spain
Enstatite							
Atlanta		EL6	Find	5.5 kg	0.035	1938	Louisiana, USA
Eagle	USNM 16441	EL6	Fall	10 kg	0.035	1946	Nebraska, USA
Khairpur		EL6	Fall	13.6 kg	0.029	1873	Punjab, Pakistan
LON94100		EL6	Find	1947 g	0.050	1994	Antarctica

and Os isotopes to 33, spanning H3 to H6, L3 to L6 and LL3 to LL6 types. The enstatite group measured in this study are all EL chondrites expanding the total number of these chondrites to 27 individual samples spanning EH3 and EL3 to EH5 to EL6. Combined with six individual Rumuruti chondrites, the total number of chondrite meteorites now studied for HSE abundances is > 100, with several of these samples analyzed multiple times, and in different laboratories (Table S1). The ordinary chondrite Chelyabinsk (LL5) was the only sample from this study to be measured for mineral chemistry (trace-, major-element, HSE), as well as bulk measurements, providing a point of comparison with mineral chemical data from other chondrite meteorites.

3. ANALYTICAL METHODS

3.1. Mineral chemistry of the Chelyabinsk meteorite

Thick sections of Chelyabinsk were prepared and polished from fragments of the meteorite delivered to L.A. Taylor in 2013. Major- and minor-element mineral compositions were measured using a *Cameca SX-100* electron probe micro analyzer at the University of Tennessee. Analyses were made using a beam size of 1 μm and an accelerating potential of 15 keV. Standards were used in the calibration of the instrument as well as throughout the analysis to confirm data quality. See Day et al., (2015) for further detail on methods and techniques used during analysis.

Silicate, phosphate, sulfide and metal phases in a polished thin section of Chelyabinsk were measured at the Scripps Isotope Geochemistry Laboratory (*SIGL*) using a *New Wave Research* UP213 laser ablation system coupled to a *Thermo Fisher Scientific* iCAP Qc inductively coupled plasma mass spectrometer (ICP-MS). A 150 μm beam diameter was used for analysis spots with a laser repetition rate of 5 Hz. Within the 3 cm^3 ablation cell in which the analysis took place, He-gas was flushed to enhance the transport and production of a fine aerosol which was then mixed with an Ar carrier-gas (~1 L/min) before reaching the plasma. Data collection occurred over a period of ~60 s with a washout time of > 120 s between each analysis. Time-resolved mode was used to account for mineral zoning, inclusions and possible underlying phases in the polished thin section. Standardization for silicates and phosphates was done relative to NIST 612, with measurement of BHVO-2g, BCR-2g and NIST 610 as unknowns. Standardization for metal and sulfide phases was performed using the iron meteorite in-house standards Filomena (North Chile), Hoba and Coahuila, the compositions of which are reported in Day et al., (2018), as well as sulfide standard MASS-1, in order to determine siderophile element abundances.

3.2. Major- and trace element abundance determination

Fragments of individual chondrites were powdered with limited force using an agate mortar and pestle. Care was taken to avoid fusion crust except in the deliberate case of analysis for a fragment of the Chelyabinsk meteorite. For large metal portions (>1 mm), no attempt was made to disaggregate these materials, due to the potential for metal smearing, so some 'nugget heterogeneity' is inevitable in prepared powders. These metal incorporations are especially visible in samples with limited mass and/or high initial metal content (e.g., CB chondrite, Gujba).

Bulk sample trace- and major-element abundance measurements (including blanks and terrestrial standards BHVO-2, BCR-2, AGV-2) were done by digesting sample powders using Teflon Paar bombs or Teflon vials at the *SIGL* (Table 4). Powders were precisely weighed, and those placed in Teflon Paar bombs were digested at 180 °C in Optima grade HF (4 mL) and HNO_3 (1 mL) for ~72 hours in a processing oven, before being dried down. Powders placed in Teflon beakers were digested in concentrated Teflon-distilled HF (4 mL) and HNO_3 (1 mL) for ~72 hours on a hotplate at 140 °C. Resulting solutions from both digestion methods were then sequentially dried and taken up in concentrated HNO_3 and HCl to destroy fluoride complexes over the course of several days. Sample stock solutions were prepared by adding 1 ml of Teflon distilled nitric acid (HNO_3), 1 ml of 1 ppm indium (In) spike and 3 ml of 18.2 Ω MQ water to each sample. For trace-element analysis, 500 μl of the prepared solution was added to clean centrifuge tubes. 10 ml of 2% nitric acid was then added to each of the centrifuge tubes to dilute the sample. Trace element abundances were measured using a *ThermoScientific* iCAP Qc ICP-MS, using established methods (Day et al., 2015).

For major element measurements, 1 ml of solution was aliquoted from each of the centrifuge tubes after trace elements analyses were completed. After discarding the remaining liquid in the centrifuge tube, the 1 ml was returned to the tube and 9 ml of 2% nitric acid was added to dilute the sample to appropriate count rates on major element isotopes (e.g., $<10^8$ cps on ^{54}Fe). Samples were then measured using the iCAP Qc ICP-MS, with Si derived by difference, assuming no total volatile content (see Tait and Day, 2018 for discussion). The reproducibility of trace elements in the reference material BHVO-2 was generally better than 4 to 9% (RSD) excluding Pb (17%), Te (15%), Mo (24%), and Se (11%). For major elements, the reproducibility of the reference material was better than 2 to 3% (RSD), except for P (7%).

3.3. Strontium isotope analysis

Strontium isotope compositions and Rb and Sr abundances were obtained using stock solutions from the major- and trace-element analysis. Calibrated Sr-specification resins loaded in home-made Teflon columns were used to separate Sr from other elements, using the method described in Tait and Day (2018). The separated Sr-cuts were loaded onto outgassed rhenium filaments and measured on the SIGL *ThermoScientific* Triton TIMS in positive ion mode. The quantitative recovery of Sr after column chemistry was 100 ± 1%, while the blank (<5 ng Sr) was negligible compared to the sample loads (typically > 0.5 μg Sr). The Sr standard solution SRM 987 (390 ng load size), gave an average $^{87}Sr/^{86}Sr$ value of 0.710241 ± 2 (n = 5). Four separate digestions of the BHVO-2 terrestrial standard gave 0.703472 ± 3 (n = 8). USGS standards AGV-2 (0.703983 ± 12, n = 3, 2SE) and BCR-2 (0.704999 ± 5, n = 2, 2SE) were also measured; the values are in good agreement with recommended values from the GEOREM database (Jochum et al., 2005) of 0.703478 ± 34 (BHVO-2), 0.703992 ± 33 (AGV-2), and 0.70492 ± 55 (BCR-2), respectively. Multiple analyses of Rb and Sr abundances were made using the iCAP Qc ICP-MS, with reliable determination of the $^{87}Rb/^{86}Sr$ ratio of aliquots with ~0.05 ppm total Rb at 6% (2SD).

3.4. Oxygen isotope analysis

Oxygen isotope analysis was performed at the Institut de Physique du Globe-Paris using identical methods to those described in Rumble et al., (1997). Oxygen isotopic ratios ($^{X}O/^{16}O$, where X = 18 or 17) are measured versus international standard, V-SMOW, and expressed in δ notation, according to the following equation: $\delta^{X}O = 1000 \times ((^{X}O/^{16}O)/(^{X}O/^{16}O_{std}) - 1)$. From the delta notation values, $\Delta^{17}O$ (in per mil, representing deviation from the terrestrial fractionation line: $\Delta^{17}O = \delta^{17}O - ((\delta^{18}O/1000 + 1)\ \hat{}\ 0.5305 - 1) \times 1000$) was calculated (Criss and Farquhar, 2008). Measurement of the San Carlos olivine and UWG-2 garnet standard aliquots gave (in per mil) uncertainties of ± 0.09 on $\delta^{17}O$, ± 0.17 on $\delta^{18}O$, and an average of $\Delta^{17}O = -0.004 \pm 0.018$ (2 SD; $n = 18$). In-run uncertainties for individual measurements were < 0.06‰ for $\delta^{17}O$ and < 0.03‰ for $\delta^{18}O$.

3.5. Highly siderophile element abundances and Os isotopes

For highly siderophile element (HSE) abundance and osmium isotope analysis, 10 cm long borosilicate Carius tubes were used for sample digestion. Precise masses of powdered sample were transferred into Carius tubes with an appropriate amount of an isotopically enriched spike (^{99}Ru, ^{106}Pd, ^{185}Re, ^{190}Os, ^{191}Ir, ^{194}Pt) and ~6 mL of double Teflon distilled 12 N HCl (2.5 mL) and 15.7 N of HNO_3 (3.5 mL) purged of Os and double Teflon distilled, before sealing the Carius tubes. Samples were digested for 72 hours at ~240 °C in a convection oven. Osmium was separated from the other HSE in samples using solvent extraction in CCl_4 and then back extraction into HBr (Cohen and Waters, 1996). The fraction of HCl-HNO_3 solution remaining from the samples was then dried down and redissolved in 1 M HCl. The HSE were separated from bulk samples using a solvent extraction and anion exchange column procedure outlined in Day et al., (2016a). Each of these fractions were then dried down before analysis using a *Cetac* Aridus II Desolvating Nebulizer coupled to a *ThermoScientific* iCAPq C ICP-MS at the *SIGL*. Iridium, Ru, Pt, Pd and Re total procedural blanks prepared with the samples had contents lower than those of the loaded sample masses by a factor of ~10,000 on average, resulting in negligible blank corrections. The osmium fractions were purified by micro-distillation into HBr from a dichromate solution in H_2SO_4 (Roy-Barman, 1993). Purified Os cuts were then measured using negative ions on the Thermo Scientific Triton thermal ionization mass spectrometer (TIMS) at the *SIGL* using established methods (Day, 2016). Total analytical blanks (TAB) for Os isotope analysis had $^{187}Os/^{188}Os$ ratios of 0.28 ± 0.11 (n = 3) and 0.2 ± 0.2 pg Os, with 1.0 ± 0.5 pg Re, 10 ± 4 pg Pd, 10 ± 5 pg Pt, 5 ± 5 pg Ru, 2 ± 2 pg Ir. These blanks represent < 1% of the total analyte in all cases and blank corrections are negligible.

4. RESULTS

4.1. Chelyabinsk meteorite fall petrography and mineral chemistry

Fragments of Chelyabinsk studied in this work are similar to the light lithology reported in other studies (Brown et al., 2013; Righter et al., 2015). The dark lithology in

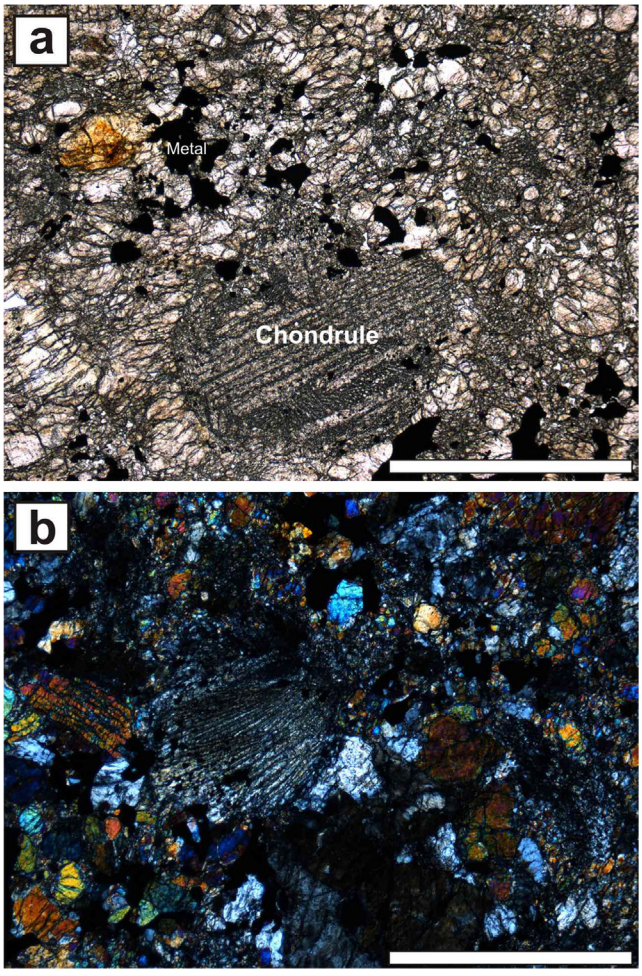

Fig. 1. a) Plane-polarised light and (b) cross-polarised light images of the Chelyabinsk ordinary chondrite, illustrating regions of metal and sulfide (rusty regions), presence of chondrules and highly equilibrated matrix material. Scale bars are 1 mm.

Table 2
Major-element mineral chemistry (wt%) for the Chelyabinsk chondrite meteorite fall, February 15th, 2013.

Phase	Olivine		Plagioclase		Orthoclase	Low-Ca Pyroxene		High-Ca Pyroxene		Cr-Spinel		Ilmenite		Apatite		Merrillite			Troilite		Kamacite	Taenite	Taenite
n	[128]	*1SD*	[60]	*1SD*	[1]	[156]	*1SD*	[55]	*1SD*	[35]	*1SD*	[6]	*1SD*	[79]	*1SD*	[32]	*1SD*		[12]	*1SD*			
SiO_2	37.5	*0.6*	65.4	*0.9*	64.8	54.9	*0.4*	53.6	*0.5*	0.08	*0.04*	0.03	*0.01*	0.10	*0.25*	0.01	*0.02*	Si	0.01	*0.00*	0.01	0.01	0.00
TiO_2	0.01	*0.01*			0.04	0.19	*0.05*	0.40	*0.06*	3.01	*0.38*	53.2	*0.4*					S	36.1	*0.22*			0.00
Al_2O_3	0.01	*0.04*	21.9	*0.7*	19.7	0.15	*0.06*	0.45	*0.05*	5.84	*0.21*	0.01	*0.01*					Fe	62.8	*0.27*	92.1	50.8	72.0
Cr_2O_3	0.04	*0.08*				0.16	*0.35*	0.70	*0.10*	56.1	*1.0*	0.09	*0.08*					Co	0.00	*0.01*	2.03	0.33	1.12
MgO	35.8	*0.6*	0.05	*0.17*	0.01	27.6	*0.3*	16.3	*0.3*	1.87	*0.32*	2.45	*0.29*	0.19		3.61	*0.07*	Ni	0.06	*0.07*	5.67	48.8	25.8
CaO	0.09	*0.68*	2.21	*0.27*	1.44	0.72	*0.13*	21.96	*0.56*	0.02	*0.03*	0.03	*0.01*	53.9	*0.9*	46.7	*0.2*	P	0.00	*0.00*			0.01
MnO	0.45	*0.02*			0.02	0.45	*0.02*	0.21	*0.02*	0.53	*0.03*	1.17	*0.26*					Mg	0.00	*0.00*	0.01		0.00
FeO	26.1	*0.6*	0.49	*0.31*	0.18	15.8	*0.2*	5.3	*0.4*	31.8	*0.4*	42.5	*0.6*	0.38	*0.38*	0.64	*0.26*	Al	0.00	*0.00*	0.00	0.01	0.01
NiO	0.01	*0.02*								0.02	*0.02*	0.04	*0.01*					Ti	0.00	*0.00*		0.01	0.00
Na_2O			8.96	*0.89*	1.02	0.01	*0.01*	0.49	*0.04*					0.05	*0.04*	2.37	*0.11*	**Total**	**99.1**	***0.5***	**99.8**	**100.0**	**99.0**
K_2O			0.97	*0.52*	14.1																		
P_2O_5	0.03	*0.05*												41.4	*0.6*	46.2	*0.4*	*Fe*	50		52	74	93
V_2O_3										0.66	*0.06*							*Ni*			48	25	5
Cl														5.35	*0.40*			*S*	50				
F														0.18	*0.14*								
SO_3														0.02	*0.02*								
Total	**100.0**	***0.7***	**99.9**	***1.0***	**101.3**	**100.0**	***0.6***	**99.3**	***1.0***	**99.9**	***1.03***	**99.5**	***0.48***	**101.6**		**99.5**							
O = Cl														1.21	*0.09*								
O = F														0.07	*0.06*								
Fo	71.0	*0.4*																					
Or			6	*3*	84																		
An			11	*2*	7																		
Ab			83	*4*	9																		
En						74.6	*0.4*	46.4	*0.5*														
Wo						1.4	*0.3*	45.1	*0.9*														
Fs						24.0	*0.4*	8.5	*0.9*														
Mg#						76		85		9.5		9.3		82		9							
Cr#										79.5													

An = Ca/(Ca + Na + K)*100, Ab = Na/(Ca + Na + K)*100, Wo = Ca/(Ca + Mg + Fe)*100, En = Mg/(Ca + Mg + Fe)*100, Mg# = Mg/(Mg + Fe)*100, Cr# = Cr/(Cr + Al)*100

the studied sample juxtaposes the fusion crust and exhibits infilling of cracks in minerals by Fe-metal veinlets. The groundmass is crystallized, but chondrules are still discernable (Fig. 1), showing variable chondrule textures. Although shock veins are present, the shock degree has not generated maskelynite or planar deformations in the examined sample. Minerals are remarkably homogenous (Table 2), and major phases are 44–49 vol% pyroxenes (mainly $Fs_{24}Wo_{1.4}$, with minor $Fs_{8.5}Wo_{45.1}$); 43–46 vol% olivine (Fa_{29}); ~10 vol% feldspars (mainly $Ab_{83}Or_6$ with minor Ab_9Or_{84}), ~4 vol% troilite (FeS), and 2–3 vol% FeNi metal. Cobalt and Ni contents of kamacite and taenite are consistent with Chelyabinsk falling in the LL field (Fig. 2). Mafic minerals are more Fe-rich than the Kunashak (L6) chondrite that fell in the same region 56 years earlier (Dunaway et al., 2006). In conjunction with the fayalite content of the olivine, which falls in the range of LL3.8-6 (Rubin, 1990), Chelyabinsk can be classified as an LL5 ordinary chondrite. The presence of sanidine ($Ab_{12}Or_{81}$) in the sample is unusual for an ordinary chondrite. It occurs as exsolution lamellae (1–2 μm thick) in albite. Minor phases include chromite, ilmenite, merrillite [$Na_{0.82}(Fe_{0.97}, Mg_{0.97},Ca_9)(PO_4)_7$], and chlorapatite [$Fe_{0.02}Ca_{4.97}(PO_4)_3(Cl_{0.78\ \pm0.06}F_{0.05\ \pm0.04})$]. Rust in the sample indicates the possible presence of lawrencite ($FeCl_2$), and its rapid oxyhydration during or after sample preparation to an iron oxyhydroxide, probably akaganéite. Energy dispersive spectroscopy of this alteration product verifies the presence of Cl, Fe, and traces of Ni. With the notable exceptions outlined above, the petrology and mineral chemistry of the sample that we examined is similar to other reported studies (Brown et al., 2013; Righter et al., 2015).

The mineral trace element data are shown in Fig. 3 and are given in Table 3. Normalized to the CI Orgueil measurements from Barrat et al., (2012), the low-Ca pyroxene (n = 8) has trace element abundances close to that of the fusion crust excluding minor anomalies for Eu and Th. The fusion crust is relatively depleted in the rare earth elements (REE), Rb, Sr, Y, Th and U compared with the bulk rock measurement aliquot without fusion crust, showing that it is not a strong representation of the bulk sample. Olivine ($n = 4$) generally shows a value ~0.1 × FC for trace elements, excluding Li and Sc. Both the chondrules ($n = 4$) and plagioclase ($n = 1$) are enriched in trace elements relative to fusion crust, the latter also showing a positive Eu anomaly. These lines of evidence suggest the fusion crust composition is strongly dominated by olivine and low-Ca pyroxene in the fractions measured in this study. The phosphate ($n = 1$) that was measured from Chelyabinsk is REE enriched (~500–1000 × fusion crust), and has high U, Th, Pb and Y, and includes a negative Eu anomaly. There are notable high field strength element (HFSE; Ti, Nb, Ta, Zr, Hf) variations in olivine, phosphate and chondrules. Abundances of the HSE in the sample metals highlight two populations where type-2 metals show a depletion in Pd and Au (<10 × CI-chondrite) compared to type-1 (> 10 × CI-chondrite), being similar to some metals in acapulcoites and lodranites (Fig. 4). Previous studies have shown that high Ni-metals tend to contain high Cu, Pd and Au relative to low-Ni metals while refractory platinum group elements remain nearly unfractionated between high and low-Ni metal groups in both chondrites and partially melted achondrites (Campbell and Humayun, 2003; Dhaliwal et al., 2017), consistent with that observed for Chelyabinsk metals.

4.2. Major elements and representativeness of studied chondrites

The major-element compositions for bulk chondrites are reported in Table 4 and shown in Fig. 5. Compared with average major-element compositional data for different chondrite meteorite groups (Alexander, 2019a,b), the new data either show good correspondence, as is the case for the enstatite chondrites, or reveal fractionation effects likely related to the small sample aliquot size used in some cases (see Table 1). For example, the new data falls along trends of variable Mg/Si for higher Al/Si in carbonaceous chondrites compared with ordinary chondrites. On the other hand, a small aliquot of Graves Nunatak (GRA) 06101 was analyzed (0.022 mg), and this sample has the highest reported Al/Si and Mg/Si of the dataset. Examining small aliquots, such as GRA 06101 has both advantages and disadvantages for examining chemical variation in chondrites. The disadvantage is that small aliquot sizes mean that the reported data in this study should not be considered as representative of the bulk meteorite. Advantages are that the sampling procedure employed enables identification of heterogeneities within the chondrites to explore the likely range of incompatible trace element and HSE variations in their components; issues that are explored in the discussion.

4.3. Trace element abundance variations in chondrite components

Trace element variations in the chondrite components examined are presented in Table 4 and Figs. 6–8. Incompatible trace element patterns for different groups of carbonaceous chondrites are shown in Fig. 6. In general, most samples within each group ($C2_{ung}$, $CK4_{an}$, CV3, CM2) show a depletion in Rb while the remaining incompatible trace elements are slightly enriched relative to CI-chondrite Orgueil (Friedrich et al., 2002). Large variations of Ba and U exist amongst the samples, most notably in the Allende aliquots. Northwest Africa (NWA) 5958 shows enrichments in Ba, U and Sr relative to CI-chondrite Orgueil (Fig. 6a). Two separate sample aliquots of Maralinga follow similar patterns excluding the Ba measurements, which vary by a factor of ~1000 (Fig. 6b). GRA 06101 is enriched in Th and the REE relative to other CV3 chondrites measured in this study, although, as noted previously, we analyzed a small aliquot of this sample (Fig. 6c). In addition to the Ba and U variations in the Allende aliquots, sample Allende UCSD 142 also shows a relatively high enrichment of La and Ce (Fig. 6c). From the CM2 samples, Murray shows the most significant enrichment of incompatible elements of all the carbonaceous chondrites measured. Both Murchison samples show an enrichment in Th, however, the Murchison fragment

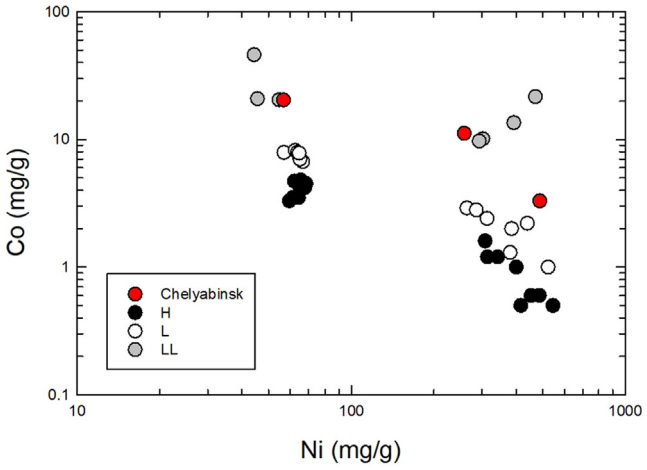

Fig. 2. Cobalt versus nickel (mg/g) in taenite and kamacite mineral phases for equilibrated H, L and LL chondrites from Afiattalab and Wasson, 1980, with Chelyabinsk data from this study shown for comparison. Compositions for taenite are on the right of the plot and kamacite compositions are on the left. The kamacite and taenite grains in Chelyabinsk fall in the range of LL ordinary chondrites. Figure after Brearley and Jones (1998).

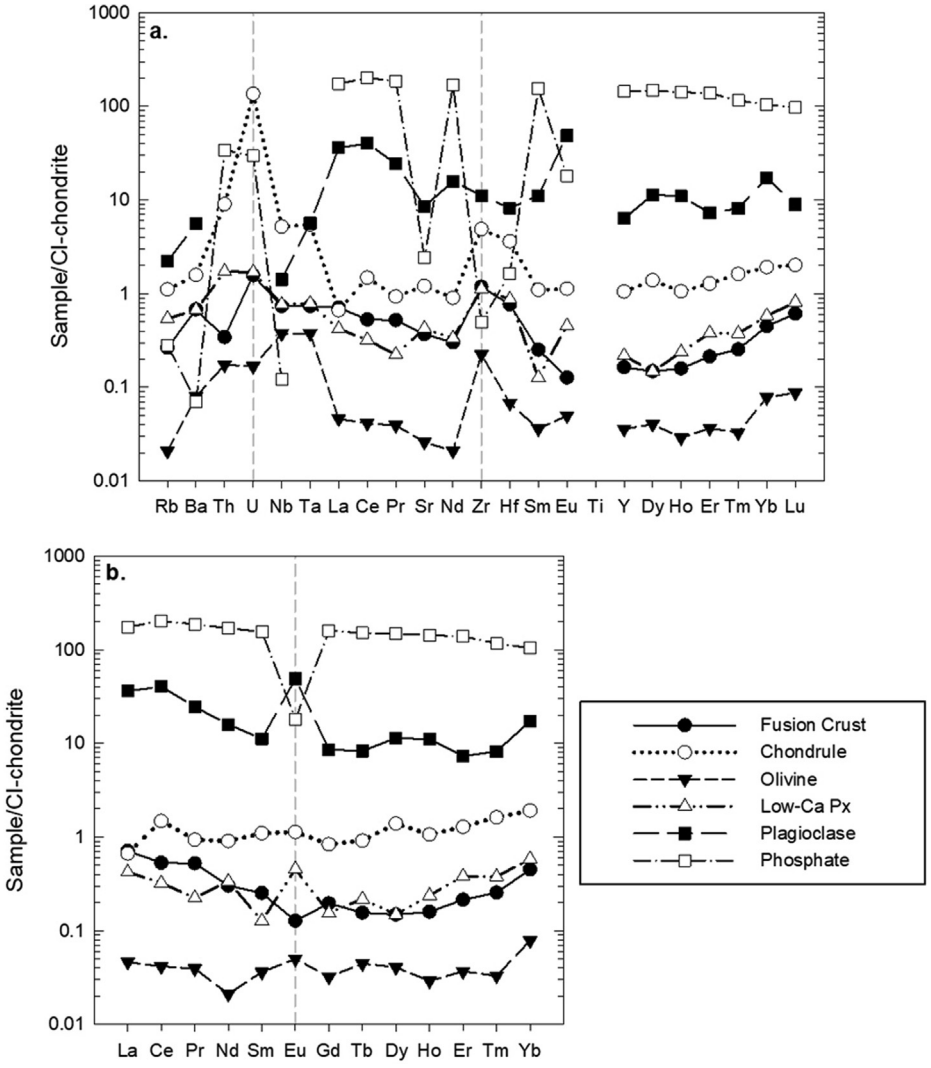

Fig. 3. (a) Incompatible trace element patterns in Chelyabinsk mineral phases, fusion crust ($n = 4$), chondrules ($n = 4$), olivine ($n = 4$), low-Ca pyroxene (Px) ($n = 8$), plagioclase ($n = 1$) and phosphate ($n = 1$). b. The rare earth element patterns for the same mineral phases mentioned above. Data are normalized to CI-chondrite Orgueil from Barrat et al., (2012).

Table 3
Trace-element mineral chemistry (ppm) for the Chelyabinsk chondrite meteorite fall, February 15th, 2013.

	Fusion Crust		Chondrule		Olivine		Low-Ca Px		Plagioclase	Phosphate		Metal 1		Metal 2	
n	[4]		[4]		[4]		[8]		[1]	[1]		[5]		[3]	
Li	1.7	0.2	0.9	0.7	1.7	0.9	0.4	0.6	1.6	0.2	Re	0.99	0.15	0.90	0.35
Sc	10.1	3.3	27.4	2.3	13.6	4.3	13.6	5.5	8.6	1.2	Os	9.48	1.70	6.40	3.56
Rb	0.65	0.96	2.71	0.38	0.051	0.003	1.32	1.30	5.40	0.69	Ir	7.40	1.03	5.54	2.90
Sr	2.7	4.1	8.9	1.6	0.2	0.0	3.2	3.2	62.7	17.8	Ru	8.50	1.81	6.35	0.88
Y	0.2	0.2	1.5	0.3	0.1	0.0	0.3	0.1	9.3	209.8	Rh	2.60	0.45	2.47	0.63
Zr	4.2	5.8	17.5	3.9	0.8	0.3	4.0	3.7	39.9	1.8	Pt	11.84	1.97	12.13	4.14
Nb	0.2	0.1	1.4	0.2	0.10	0.05	0.2	0.1	0.4	0.0	Pd	12.10	2.24	1.47	0.35
Cs	0.032	0.004	0.46	0.28	0.006	0.015	0.014	0.006		0.46	Au	2.90	0.68	0.74	0.23
Ba	1.7	2.4	3.8	1.0	0.2	0.1	1.6	1.6	13.5	0.2					
La	0.16	0.22	0.15	0.06	0.010	0.015	0.096	0.124	8.21	39.6					
Ce	0.31	0.41	0.86	0.59	0.024	0.030	0.188	0.148	23.38	117.7					
Pr	0.05	0.05	0.08	0.04	0.003	0.004	0.020	0.015	2.16	16.4					
Nd	0.14	0.19	0.40	0.24	0.009	0.009	0.150	0.222	7.10	75.5					
Sm	0.04	0.04	0.16	0.03	0.005	0.005	0.019	0.020	1.64	22.8					
Eu	0.01	0.01	0.06	0.01	0.003	0.004	0.025	0.031	2.72	1.0					
Gd	0.04	0.03	0.17	0.02	0.006	0.007	0.031	0.033	1.69	31.6					
Tb	0.01	0.00	0.03	0.01	0.002	0.001	0.008	0.007	0.30	5.4					
Dy	0.04	0.03	0.34	0.07	0.010	0.010	0.036	0.016	2.76	36.0					
Ho	0.01	0.01	0.06	0.01	0.002	0.000	0.013	0.004	0.59	7.6					
Er	0.03	0.02	0.20	0.03	0.006	0.004	0.061	0.032	1.16	22.0					
Tm	0.01	0.00	0.04	0.01	0.001	0.000	0.009	0.004	0.20	2.9					
Yb	0.07	0.02	0.31	0.14	0.013	0.001	0.093	0.033	2.75	16.7					
Lu	0.01	0.00	0.05	0.01	0.002	0.002	0.019	0.007	0.21	2.2					
Hf	0.08	0.12	0.39	0.01	0.007	0.005	0.094	0.090	0.89	0.2					
Ta	0.01	0.01	0.08	0.01	0.005	0.001	0.011	0.005	0.08	BDL					
Pb	0.04	0.03	0.19	0.02	BDL	BDL	0.053	0.063	BDL	0.30					
Th	0.01	0.00	0.25	0.10	0.005	0.006	0.047	0.027	BDL	0.94					
U	0.01	0.02	1.02	1.40	0.001	0.003	0.013	0.012	BDL	0.22					

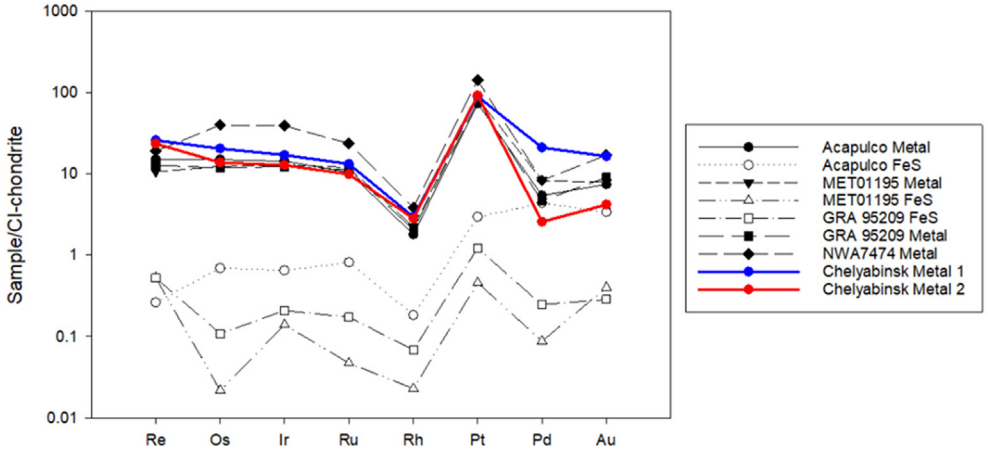

Fig. 4. Highly siderophile element abundances in Chelyabinsk metals, Type-1 ($n = 5$) in blue and Type-2 ($n = 3$) in red. Acapulco, MET01195, GRA95209 and NWA7474 metal and FeS abundances from Dhaliwal et al., (2017). CI-chondrite normalization from compilation in Day et al., (2016a). (For interpretation of the references to colour in this figure legend, the reader is referred to the web version of this article.)

shows far more variability in its measurements of incompatible elements; enrichments also occur in Ba, U, Zr, Hf, Ti and Lu (Fig. 6d).

Incompatible trace element variability between different groups of ordinary chondrites are shown in Fig. 7. Both the Chelyabinsk samples (LL5) - one containing fusion crust and the other without - show similar patterns in their incompatible trace elements, however the Chelyabinsk sample without fusion crust is slightly more enriched in the incompatible trace elements than the sample with fusion crust (Fig. 7a). As noted previously, while the incompatible trace element compositions between the Chelyabinsk sam-

Table 4
Bulk-rock major, minor and trace-element chemistry for the Chelyabinsk chondrite meteorite fall and other chondrites.

Sample	Type	Method[a]	Na wt.%	Mg wt.%	Fe wt.%	Al wt.%	P wt.%	Ca wt.%	Ti wt.%	Mn wt.%	Cr wt.%	Co wt.%	Ni wt.%
Ordinary													
Chelyabinsk (With FC)	LL5	[1]	0.610	12.16	22.85	0.97	0.11	1.08	0.05	0.21	0.34	0.17	1.90
Chelyabinsk (Without FC)	LL5	[1]	0.609	12.58	17.11	0.96	0.12	1.30	0.07	0.23	0.30	0.05	1.35
Olivenza	LL5	[2]							0.05	0.26	0.28	0.05	1.06
Saratov	L4	[2]	0.62	13.63	16.52	0.98	0.09	1.68	0.05	0.31	0.30	0.04	0.79
Saratov	L4	[2]	0.46	11.44	15.45	0.87	0.07	1.02	0.04	0.18	0.28	0.04	0.97
Saratov	L4	[2]							0.06	0.26	0.37	0.05	1.27
NWA869	L3-6	[1]	0.76	14.09	19.47	1.30	0.28	1.79	0.13	0.24	0.28	0.03	1.12
NWA869	L3-6	[2]	0.69	12.61	19.48	1.16	0.09	1.54	0.05	0.23	0.28	0.03	1.25
AÏr	L6	[2]	0.75	15.27	19.45	1.16	0.10	1.90	0.08	0.26	0.33	0.03	0.60
AÏr	L6	[2]							0.07	0.25	0.34	0.06	1.36
AÏr	L6	[2]	0.64	12.38	20.15	0.99	0.07	1.12	0.06	0.23	0.30	0.05	1.26
Kunashak (Slice)	L6	[1]	0.65	13.14	16.66	1.05	0.11	1.34	0.07	0.23	0.32	0.03	0.68
Kunashak (Fragment)	L6	[1]	0.63	12.93	16.79	1.02	0.10	1.27	0.07	0.23	0.30	0.04	0.82
Khohar	L3.6	[2]							0.05	0.23	0.32	0.09	1.68
Kyle	L6	[2]	0.61	14.19	19.14	1.11	0.10	1.71	0.06	0.25	0.33	0.04	0.75
Kyle	L6	[2]	0.59	12.60	18.36	1.13	0.10	1.23	0.05	0.23	0.32	0.05	1.08
Peace River (Fragment)	L6	[1]	0.74	15.21	17.72	1.25	0.11	1.46	0.09	0.27	0.33	0.04	0.87
Fayateville	H4	[2]	0.55	11.80	29.64	0.87	0.12	1.12	0.05	0.21	0.34	0.10	1.97
Pultusk	H5	[2]	0.61	12.64	32.69	1.00	0.12	1.61	0.05	0.21	0.33	0.09	1.49
Pultusk	H5	[2]							0.05	0.22	0.34	0.11	1.98
Forest City	H5	[2]	0.70	14.53	24.34	1.12	0.13	1.80	0.06	0.25	0.33	0.05	1.08
Forest City	H5	[2]							0.06	0.26	0.36	0.03	0.98
Richardton (Fragment)	H5	[1]	0.68	14.35	27.90	1.10	0.24	1.31	0.11	0.23	0.36	0.09	1.74
Carbonaceous													
Ivuna	CI	[1]			26.90		0.26		0.04	0.25	0.23	0.06	1.23
Ivuna	CI	[1]			26.52		0.26		0.03	0.25	0.23	0.06	1.19
Tagish Lake	$C2_{ung}$	[2]	0.48	11.94	20.90	1.13	0.10	1.70	0.06	0.17	0.27	0.04	0.76
NWA5958	$C2_{ung}$	[2]	0.21	11.10	20.95	1.15	0.11	1.37	0.06	0.21	0.25	0.04	0.83
NWA5958	$C2_{ung}$	[1]			28.06		0.24		0.05	0.21	0.25	0.06	1.20
Banten	CM2	[2]	0.45	11.99	21.22	1.14	0.11	1.82	0.06	0.17	0.28	0.04	0.87
Banten	CM2	[2]	0.38	9.54	18.34	0.97	0.10	1.19	0.05	0.14	0.26	0.05	1.13
Murray	CM2	[2]	0.31	11.23	19.21	1.36	0.10	1.89	0.08	0.21	0.24	0.04	0.79
Murchison (MTF 2005)	CM2	[1]	0.25	9.78	16.44	0.93	0.10	1.16	0.06	0.13	0.22	0.04	0.82
Murchison (Fragment)	CM2	[1]	0.42	11.76	22.57	1.25	0.34	1.51	0.14	0.17	0.30	0.06	1.13
Allende (UCSD 142)	CV3	[1]	0.32	12.54	20.73	1.38	0.09	1.49	0.07	0.13	0.30	0.06	1.12
Allende	CV3	[2]	0.31	12.83	21.63	1.39	0.10	1.61	0.07	0.12	0.32	0.06	1.35
Allende (Literature)	CV3		*0.34*	*15.40*	*22.10*	*1.74*	*0.11*	*2.00*	*0.10*	*0.15*	*0.36*	*0.06*	*1.37*
GRA06101	CV3	[2]	0.53	15.63	20.84	2.17	0.11	4.02	0.11	0.19	0.28	0.04	0.89
Maralinga	$CK4_{an}$	[2]	0.29	14.19	22.95	1.49	0.12	3.75	0.08	0.13	0.31	0.03	0.27
Maralinga	$CK4_{an}$	[2]	0.28	12.45	22.41	1.28	0.12	3.67	0.08	0.12	0.33	0.04	0.41
Enstatite													
LON91400	EL6	[2]	0.56	13.92	24.13	0.95	0.14	1.19	0.04	0.11	0.21	0.06	1.01
Eagle	EL6	[2]	0.62	13.92	24.48	1.05	0.11	0.86	0.04	0.19	0.16	0.06	1.09
Atlanta	EL6	[2]	0.68	14.74	16.65	1.25	0.17	0.69	0.06	0.17	0.31	0.06	1.12

Khaipur	EL6	[2]	0.51	12.15	28.28	0.73	0.12	1.08	0.06	0.13	0.22	0.07	1.24
Khaipur	EL6	[2]							0.04	0.14	0.25	0.09	1.81
Standards and TPBs													
BHVO-2	[1]	Av.	1.63	4.35	8.58	7.05	0.12	8.10	1.59	0.13	0.03	0.004	0.011
(n = 3)		RSD	3%	3%	3%	4%	7%	2%	5%	3%	3%	4%	5%
BHVO-2	[2]	Av.	1.64	4.36	8.63	7.16	0.12	8.17	1.63	0.13	0.03	0.005	0.012
(n = 4)		RSD	2%	2%	2%	1%	7%	2%	2%	2%	2%	2%	2%
		Rec.	*1.64*	*4.36*	*8.63*	*7.16*	*0.12*	*8.17*	*1.63*	*0.13*	*0.03*	*0.005*	*0.012*
BCR-2	[1]	Av.	2.13	2.02	9.11	6.58	0.16	4.78	1.27	0.14	0.003	0.004	0.002
(n = 3)		RSD	6%	5%	5%	5%	5%	5%	7%	5%	5%	5%	6%
BCR-2	[2]	Av.	2.32	2.14	9.49	6.99	0.16	5.06	1.29	0.15	0.002	0.004	0.001
(n = 3)		RSD	4%	4%	4%	4%	8%	4%	5%	4%	4%	4%	5%
		Rec.	*2.34*	*3.59*	*9.65*	*7.14*	*0.15*	*5.09*	*1.35*	*0.15*	*0.002*	*0.004*	
BIR-1	[1]	Av.	1.29	5.68	7.86	7.95	0.11	9.27	0.57	0.13	0.04	0.01	0.02
(n = 3)		RSD	4%	4%	4%	4%	7%	4%	5%	3%	3%	4%	5%
		Rec.	*1.35*	*5.85*	*7.90*	*8.20*		*9.51*		*0.14*	*0.04*	*0.01*	*0.02*
TPB (n = 4)	[1]	Av.	0.0367	0.0089	0.0437	0.0113	0.0107	0.0122	0.0512	0.0010	0.0013	0.0001	0.0013
TPB (n = 3)	[2]	Av.	0.00842	0.01143	0.00031	0.37970	0.00406	0.01937	0.00001	0.00003	0.00005	0.00002	0.00001

Sample	Type	Method[a]	Li µg/g	Sc µg/g	V µg/g	Cu µg/g	Zn µg/g	Ga µg/g	Ge µg/g	Se µg/g	Rb µg/g	Sr µg/g	Y µg/g	Zr µg/g	Nb µg/g	Mo µg/g	Sn µg/g	Cs µg/g
Ordinary																		
Chelyabinsk (With FC)	LL5	[1]	1.5	5.7	56.7	109.7	46.8	4.96	9.25	0.50	2.67	10.1	2.62	4.22	0.28	1.32	0.66	0.014
Chelyabinsk (Without FC)	LL5	[1]	1.6	6.4	51.7	85.7	38.5	4.40	5.01	0.40	2.72	10.0	3.36	4.87	0.41	0.93	0.58	0.015
Olivenza	LL5	[2]	1.8	6.9	54.9	71.4	40.3	4.35	3.87	0.36	2.60	7.5	1.80	3.78	0.28	BDL	3.41	0.163
Saratov	L4	[2]	1.5	6.2	78.6	62.8	49.7	5.09	2.10	0.09	3.12	7.9	1.77	12.63	0.31	0.57	0.35	0.188
Saratov	L4	[2]	1.3	4.1	45.4	43.9	39.3	4.08	1.64	0.27	2.00	8.2	1.63	4.59	0.26	0.51	0.22	0.156
Saratov	L4	[2]	1.8	8.3	65.5	73.6	64.3	6.07	4.32	0.41	3.56	10.9	2.11	5.10	0.40	0.45	0.72	0.195
NWA869	L3-6	[1]	3.9	8.7	86.6	84.9	44.4	5.30	1.99	0.55	2.65	60.0	1.53	9.27	0.40	0.77	0.24	0.011
NWA869	L3-6	[2]	3.3	6.1	57.8	87.2	39.0	4.89	1.65	0.34	2.04	55.2	1.41	6.09	0.38	0.72	0.28	0.010
AÏr	L6	[2]	1.9	8.1	90.4	66.5	49.4	4.94	2.15	0.44	0.65	10.4	1.84	9.67	0.55	0.81	0.31	0.002
AÏr	L6	[2]	1.7	7.8	61.0	89.7	52.4	5.64	4.78	0.70	0.65	10.1	1.66	4.99	0.52	0.61	0.86	0.002
AÏr	L6	[2]	1.6	5.4	57.7	72.3	41.1	4.85	2.14	0.20	0.50	9.6	1.51	5.90	0.48	0.92	0.29	0.002
Kunashak (Slice)	L6	[1]	1.7	7.4	56.0	52.2	29.0	4.51	3.27	0.45	1.18	10.8	1.76	5.69	0.40	0.73	0.39	0.006
Kunashak (Fragment)	L6	[1]	1.6	7.0	53.9	53.7	28.7	4.54	3.64	0.36	1.51	10.5	2.06	5.50	0.38	1.22	0.29	0.008
Khohar	L3.6	[2]	1.6	6.5	486.7	56.5	106.1	40.11	7.05	5.89	0.78	4.4	8.47	3.55	0.36	BDL	2.85	0.479
Kyle	L6	[2]	1.8	7.7	88.2	67.6	53.6	5.19	2.38	0.37	2.60	9.1	2.27	9.91	0.43	0.89	0.27	0.059
Kyle	L6	[2]	0.6	7.6	58.1	61.8	45.7	4.69	2.66	0.60	2.12	8.6	2.08	5.31	0.40	0.71	0.25	0.053
Peace River (Fragment)	L6	[1]	2.0	9.0	68.6	55.1	52.1	4.93	4.09	0.29	2.79	12.0	2.03	6.55	0.49	0.79	0.39	0.008
Fayateville	H4	[2]	1.5	4.4	57.7	76.9	39.6	5.41	4.83	0.55	1.87	8.3	1.66	4.67	0.34	1.25	0.98	0.08
Pultusk	H5	[2]	1.6	6.8	85.5	82.9	42.4	6.81	3.63	0.37	2.70	9.0	1.85	6.83	0.36	1.72	0.33	0.188
Pultusk	H5	[2]	1.5	7.0	59.1	91.5	44.7	6.54	6.63	0.60	2.73	9.6	1.80	4.41	0.37	1.16	0.83	0.165
Forest City	H5	[2]	1.9	7.7	89.8	89.9	46.1	5.51	2.64	0.47	2.88	10.1	2.17	10.72	0.42	1.26	0.24	0.101
Forest City	H5	[2]	1.9	8.5	65.5	87.7	41.5	5.00	2.83	0.79	3.08	11.0	2.27	5.53	0.45	0.68	0.66	0.090
Richardton (Fragment)	H5	[1]	1.7	7.8	69.3	99.8	68.4	6.82	6.40	0.48	2.81	10.8	2.04	5.79	0.40	1.43	0.65	0.056
Carbonaceous																		
Ivuna	CI	[1]	1.4	6.1	45.1	115.4	408.8	11.04	24.38	1.46	2.36	5.6	1.70	3.70	0.30	1.33	1.63	0.251
Ivuna	CI	[1]	1.4	6.0	44.1	113.6	405.2	10.72	23.19	1.44	2.37	5.5	1.60	3.52	0.30	1.28	1.66	0.245
Tagish Lake	$C2_{ung}$	[2]	1.7	7.2	82.3	103.1	142.3	8.23	2.47	0.58	1.57	11.1	1.97	9.97	0.37	1.11	0.84	0.129
NWA5958	$C2_{ung}$	[2]	2.2	5.9	83.2	114.7	169.5	7.77	3.67	0.35	0.77	32.6	1.89	7.23	0.32	1.41	0.98	0.075
NWA5958	$C2_{ung}$	[1]	2.4	8.0	58.1	93.0	224.3	8.45	14.69	0.52	0.80	27.7	2.25	4.50	0.35	1.47	0.99	0.087
Banten	CM2	[2]	1.6	7.4	88.8	125.0	149.8	8.02	2.32	0.56	1.74	10.1	2.06	10.46	0.39	1.26	2.58	0.136
Banten	CM2	[2]	1.4	7.5	57.9	109.2	131.2	6.91	2.34	0.85	1.31	9.0	1.93	4.85	0.34	0.93	2.21	0.102
Murray	CM2	[2]	3.01	6.4	87.0	106.4	145.8	7.77	2.79	0.43	5.05	19.7	3.60	37.09	1.36	1.11	0.96	0.290
Murchison (MTF 2005)	CM2	[1]	1.3	5.6	42.4	81.7	115.9	5.99	6.63	0.54	1.30	10.8	1.80	4.20	0.29	0.97	0.78	0.104

Murchison (Fragment)	CM2	[1]		1.6	7.2	70.0	115.2	152.4	8.00	8.88	0.69	2.33	10.6	2.34	8.05	0.39	1.85	1.11	0.128
Allende (UCSD 142)	CV3	[1]		1.5	7.9	58.9	88.9	74.9	4.85	5.74	0.46	1.16	13.4	2.12	5.60	0.43	1.72	0.64	0.076
Allende	CV3	[2]		1.5	6.3	75.5	85.2	77.3	4.98	2.53	0.56	0.89	12.6	2.24	5.64	0.46	1.26	0.48	0.072
Allende (Literature)	CV3			*1.40*	*11.0*	*82.4*	*97.0*	*106.0*	*5.90*	*17.90*		*1.32*	*15.7*	*2.63*	*6.77*	*0.57*	*1.45*	*0.30*	*0.098*
GRA06101	CV3	[2]		1.72	12.2	156.9	70.1	77.2	5.08	2.57	0.17	1.18	21.3	3.39	19.58	0.51	1.51	0.58	0.065
Maralinga	$CK4_{an}$	[2]		1.87	9.3	110.1	51.8	51.7	4.46	2.50	0.09	0.59	31.3	2.47	10.64	0.49	0.67	0.35	0.021
Maralinga	$CK4_{an}$	[2]		1.57	5.2	79.4	50.7	45.4	4.27	1.79	0.16	0.43	29.8	2.13	5.79	0.46	0.57	0.31	0.109
Enstatite																			
LON91400	EL6	[2]		1.62	7.1	53.5	83.0	4.9	12.73	2.67	0.57	2.11	7.2	1.27	7.99	0.20	0.95	0.39	0.113
Eagle	EL6	[2]		1.23	6.2	38.3	52.6	164.9	13.54	3.48	0.21	2.03	6.7	1.24	3.72	0.11	0.90	0.86	0.154
Atlanta	EL6	[2]		1.26	6.3	63.2	63.8	50.0	12.82	2.01	0.41	1.38	8.5	1.87	12.96	0.26	1.17	1.10	0.052
Khaipur	EL6	[2]		1.62	4.8	56.6	84.1	12.6	14.49	3.67	0.43	1.54	4.9	1.05	6.06	0.20	1.05	0.82	0.079
Khaipur	EL6	[2]		1.65	6.2	43.8	95.6	0.7	15.09	10.91	0.86	1.69	6.3	1.26	3.33	0.24	0.16	2.07	0.077
Standards and TPBs																			
BHVO-2		[1]	Av.	4.69	31.8	317.4	128.1	104.1	22.10	1.64	0.11	9.95	403.8	25.83	170.3	18.03	3.71	1.84	0.10
(n = 3)			RSD	3%	4%	6%	5%	5%	5%	6%	2%	3%	3%	3%	3%	2%	28%	6%	3%
BHVO-2		[2]	Av.	4.80	32.0	317.0	127.0	103.0	22.00	1.60	0.17	9.11	396.0	26.00	172.0	18.10	4.00	1.70	0.10
(n = 4)			RSD	3%	3%	2%	2%	7%	2%	4%	11%	1%	1%	1%	2%	2%	24%	3%	1%
			Rec.	*4.80*	*32*	*317*	*127.0*	*103.0*	*22.00*	*1.60*	*0.10*	*9.11*	*396.0*	*26.00*	*172.0*	*18.10*	*4.00*	*1.70*	*0.10*
BCR-2		[1]	Av.	9.11	31.0	387.3	19.2	122.0	21.26	1.66	0.11	47.14	323.1	33.04	173.7	11.49	232.36	2.30	1.07
(n = 3)			RSD	2%	4%	7%	7%	5%	5%	8%	4%	3%	3%	3%	3%	3%	2%	7%	2%
BCR-2		[2]	Av.	9.78	32.7	406.5	19.5	119.8	22.39	1.82	0.18	45.23	333.7	34.84	181.3	11.84	242.19	1.89	1.16
(n = 3)			RSD	5%	5%	4%	4%	3%	4%	4%	8%	4%	4%	5%	5%	6%	16%	3%	5%
			Rec.	*9.00*	*33.0*	*416*	*19.0*	*127.0*	*23.00*			*48.00*	*346.0*	*37.00*	*188.0*		*248.00*		*1.10*
BIR-1		[1]	Av.	3.28	43.1	318.0	115.2	66.7	15.45	1.22	0.02	0.21	108.2	15.2	14.6	0.52	0.038	0.80	0.01
(n = 3)			RSD	5%	6%	9%	8%	8%	7%	10%	24%	4%	5%	5%	5%	5%	29%	4%	4%
			Rec.	*3.60*	*44*	*310*	*125*	*70*	*16*				*110*	*16*	*18*	*0.60*			
TPB (n = 4)		[1]	Av.	0.017	0.081	0.350	0.312	1.370	0.003	0.011	0.043	0.005	0.021	0.001	0.062	0.002	0.026	0.277	0.001
TPB (n = 3)		[2]	Av.	0.004	0.058	0.013	0.027	3.558	0.002	0.023	0.012	0.005	0.211	0.014	1.331	0.008	0.005	0.024	0.0004

Sample	Type	Method[a]	Ba µg/g	La µg/g	Ce µg/g	Pr µg/g	Nd µg/g	Sm µg/g	Eu µg/g	Gd µg/g	Tb µg/g	Dy µg/g	Ho µg/g	Er µg/g	Tm µg/g	Yb µg/g
Ordinary																
Chelyabinsk (With FC)	LL5	[1]	3.36	0.518	1.36	0.176	0.859	0.272	0.073	0.353	0.064	0.446	0.096	0.283	0.042	0.264
Chelyabinsk (Without FC)	LL5	[1]	3.56	0.595	1.69	0.234	1.167	0.365	0.080	0.472	0.087	0.617	0.132	0.384	0.056	0.351
Olivenza	LL5	[2]	38.99	0.224	0.58	0.095	0.482	0.183	0.075	0.230	0.041	0.311	0.066	0.213	0.031	0.221
Saratov	L4	[2]	2.96	0.272	0.71	0.105	0.539	0.167	0.066	0.226	0.046	0.309	0.067	0.203	0.033	0.206
Saratov	L4	[2]	2.97	0.267	0.62	0.106	0.522	0.165	0.066	0.227	0.042	0.306	0.066	0.201	0.031	0.206
Saratov	L4	[2]	24.30	0.331	0.85	0.126	0.636	0.209	0.088	0.270	0.050	0.359	0.081	0.232	0.034	0.259
NWA869	L3-6	[1]	191.92	0.269	0.70	0.099	0.490	0.156	0.121	0.204	0.038	0.272	0.060	0.182	0.028	0.199
NWA869	L3-6	[2]	187.81	0.250	0.62	0.091	0.448	0.154	0.125	0.199	0.035	0.251	0.057	0.174	0.026	0.185
AÏr	L6	[2]	4.03	0.276	0.73	0.110	0.547	0.179	0.079	0.245	0.045	0.320	0.069	0.207	0.032	0.223
AÏr	L6	[2]	3.20	0.244	0.64	0.096	0.514	0.170	0.078	0.206	0.042	0.289	0.064	0.193	0.029	0.199
AÏr	L6	[2]	4.58	0.242	0.62	0.096	0.472	0.145	0.075	0.201	0.038	0.273	0.062	0.181	0.028	0.196
Kunashak (Slice)	L6	[1]	3.63	0.519	1.40	0.115	0.549	0.176	0.076	0.232	0.044	0.313	0.068	0.209	0.032	0.217
Kunashak (Fragment)	L6	[1]	3.79	0.378	1.03	0.135	0.647	0.214	0.075	0.274	0.052	0.365	0.080	0.239	0.036	0.241
Khohar	L3.6	[2]	1.12	0.262	0.69	0.113	0.554	0.189	0.073	0.258	0.049	0.344	0.071	0.213	0.033	0.233
Kyle	L6	[2]	4.19	0.352	0.94	0.142	0.696	0.228	0.082	0.305	0.055	0.401	0.085	0.257	0.037	0.253
Kyle	L6	[2]	3.31	0.319	0.84	0.128	0.658	0.219	0.076	0.280	0.050	0.370	0.079	0.235	0.036	0.236
Peace River (Fragment)	L6	[1]	8.07	0.301	0.81	0.118	0.592	0.193	0.084	0.259	0.048	0.345	0.075	0.229	0.035	0.234
Fayateville	H4	[2]	3.911	0.28	0.719	0.110	0.542	0.178	0.069	0.229	0.043	0.303	0.066	0.197	0.028	0.205
Pultusk	H5	[2]	3.17	0.293	0.77	0.117	0.587	0.182	0.071	0.240	0.044	0.321	0.070	0.212	0.031	0.210
Pultusk	H5	[2]	3.20	0.275	0.73	0.110	0.545	0.181	0.066	0.229	0.043	0.301	0.065	0.202	0.030	0.212

Forest City	H5	[2]	3.46	0.334	0.88	0.128	0.657	0.220	0.078	0.286	0.053	0.373	0.082	0.243	0.037	0.244
Forest City	H5	[2]	3.93	0.340	0.90	0.136	0.691	0.226	0.083	0.280	0.055	0.394	0.087	0.255	0.039	0.262
Richardton (Fragment)	H5	[1]	3.64	0.302	0.82	0.123	0.605	0.199	0.074	0.247	0.048	0.342	0.075	0.224	0.033	0.224
Carbonaceous																
Ivuna	CI	[1]	4.26	0.226	0.58	0.087	0.470	0.156	0.052	0.231	0.040	0.281	0.061	0.186	0.029	0.186
Ivuna	CI	[1]	4.23	0.226	0.55	0.084	0.443	0.147	0.050	0.219	0.041	0.271	0.061	0.185	0.028	0.180
Tagish Lake	$C2_{ung}$	[2]	4.11	0.317	0.81	0.124	0.628	0.204	0.078	0.261	0.050	0.359	0.076	0.216	0.033	0.234
NWA5958	$C2_{ung}$	[2]	27.28	0.386	0.88	0.146	0.738	0.217	0.083	0.265	0.050	0.342	0.070	0.221	0.034	0.251
NWA5958	$C2_{ung}$	[1]	35.64	0.373	0.85	0.138	0.694	0.225	0.077	0.554	0.056	0.382	0.081	0.250	0.037	0.247
Banten	CM2	[2]	3.29	0.368	0.94	0.139	0.684	0.213	0.083	0.283	0.051	0.357	0.076	0.229	0.036	0.240
Banten	CM2	[2]	3.01	0.749	1.83	0.238	0.944	0.180	0.069	0.279	0.047	0.335	0.073	0.219	0.031	0.200
Murray	CM2	[2]	40.63	2.358	5.59	0.674	2.734	0.632	0.166	0.638	0.099	0.632	0.134	0.409	0.063	0.420
Murchison (MTF 2005)	CM2	[1]	3.03	0.441	1.49	0.120	0.589	0.179	0.069	0.244	0.045	0.313	0.071	0.209	0.031	0.203
Murchison (Fragment)	CM2	[1]	34.22	0.345	0.89	0.129	0.656	0.203	0.085	0.267	0.049	0.347	0.074	0.231	0.034	0.228
Allende (UCSD 142)	CV3	[1]	4.27	1.097	5.44	0.213	1.071	0.281	0.090	0.366	0.062	0.411	0.081	0.241	0.044	0.267
Allende	CV3	[2]	7.59	0.435	1.09	0.175	0.864	0.284	0.109	0.331	0.064	0.428	0.089	0.271	0.047	0.299
Allende (Literature)	CV3		*4.74*	*0.490*	*1.24*	*0.192*	*0.967*	*0.313*	*0.115*	*0.401*	*0.072*	*0.479*	*0.100*	*0.299*	*0.053*	*0.319*
GRA06101	CV3	[2]	5.00	0.610	1.56	0.243	1.184	0.371	0.160	0.496	0.092	0.612	0.130	0.364	0.061	0.404
Maralinga	$CK4_{an}$	[2]	25.71	0.731	2.68	0.240	1.136	0.314	0.110	0.377	0.067	0.460	0.098	0.279	0.046	0.301
Maralinga	$CK4_{an}$	[2]	0.02	0.61	1.970	0.202	0.959	0.286	0.103	0.358	0.060	0.403	0.089	0.261	0.042	0.276
Enstatite																
LON91400	EL6	[2]	1.89	0.144	0.39	0.061	0.308	0.104	0.043	0.135	0.027	0.189	0.043	0.130	0.021	0.149
Eagle	EL6	[2]	2.47	0.117	0.35	0.058	0.282	0.099	0.040	0.143	0.024	0.197	0.046	0.132	0.022	0.153
Atlanta	EL6	[2]	4.80	0.227	0.69	0.108	0.599	0.178	0.051	0.242	0.045	0.317	0.066	0.203	0.028	0.195
Khaipur	EL6	[2]	1.50	0.121	0.33	0.055	0.274	0.086	0.038	0.133	0.023	0.174	0.035	0.116	0.016	0.129
Khaipur	EL6	[2]	0.27	0.122	0.35	0.063	0.288	0.099	0.039	0.133	0.024	0.199	0.042	0.131	0.020	0.144
Standards and TPBs																
BHVO-2		[1]	Av.	139.21	15.13	37.20	5.33	24.35	6.04	2.06	6.21	0.92	5.29	0.97	2.53	0.33	1.99
(n = 3)			RSD	2%	2%	2%	3%	3%	3%	3%	2%	3%	3%	3%	3%	3%	3%
BHVO-2		[2]	Av.	131.00	15.20	37.50	5.35	24.50	6.07	2.07	6.24	0.92	5.31	0.98	2.54	0.33	2.00
(n = 4)			RSD	2%	1%	1%	1%	1%	1%	2%	2%	2%	1%	1%	2%	2%	2%
			Rec.	*131.00*	*15.20*	*37.50*	*5.35*	*24.50*	*6.07*	*2.07*	*6.24*	*0.33*	*5.31*	*0.98*	*2.54*	*0.33*	*2.00*
BCR-2		[1]	Av.	653.40	22.96	48.88	6.33	26.46	6.04	1.94	6.38	0.96	5.92	1.19	3.38	0.48	3.10
(n = 3)			RSD	2%	1%	1%	1%	1%	1%	2%	2%	2%	2%	1%	1%	2%	2%
BCR-2		[2]	Av.	491.12	24.27	48.93	6.64	27.95	6.36	2.01	6.71	1.00	6.28	1.26	3.55	0.50	3.26
(n = 3)			RSD	4%	4%	1%	4%	5%	4%	3%	5%	5%	5%	5%	4%	6%	4%
			Rec.	*683.00*	*25.00*	*53.00*	*6.80*	*28.00*	*6.70*	*2.00*	*6.80*	*1.07*		*1.33*		*0.54*	*3.50*
BIR-1		[1]	Av.	6.76	0.60	1.93	0.36	2.32	1.06	0.50	1.64	0.33	2.49	0.55	1.64	0.24	1.60
(n = 3)			RSD	4%	0.3%	1%	3%	4%	4%	5%	4%	4%	4%	4%	4%	4%	4%
			Rec.	*7.00*	*0.63*	*1.90*		*2.50*	*1.10*	*0.55*	*1.80*		*4.00*				*1.70*
TPB (n = 4)		[1]	Av.	0.033	0.015	0.035	0.0008	0.0028	0.0001	0.0001	0.0005	0.0001	0.0002	0.00003	0.0001	0.00003	0.0001
TPB (n = 3)		[2]	Av.	0.042	0.002	0.006	0.0008	0.0034	0.0004	0.0002	0.0006	0.0001	0.0005	0.00008	0.0003	0.00006	0.0001

Sample	Type	Method[a]	Lu	Hf	Ta	W	Pb	Th	U	Cd
			µg/g	µg/g	µg/g	µg/g	µg/g	µg/g	µg/g	ng/g
Ordinary										
Chelyabinsk (With FC)	LL5	[1]	0.037	0.118	0.018	0.338	0.022	0.033	0.085	2.1
Chelyabinsk (Without FC)	LL5	[1]	0.051	0.147	0.032	0.532	0.034	0.049	0.121	2.2
Olivenza	LL5	[2]	0.034	0.094	0.018	0.192	0.900	BDL	0.009	
Saratov	L4	[2]	0.031	0.242	0.040	0.132	0.055	0.091	0.010	0.026
Saratov	L4	[2]	0.030	0.135	0.014	0.074	0.064	0.040	0.009	0.001
Saratov	L4	[2]	0.037	0.158	0.022	0.110	0.090	0.037	0.013	
NWA869	L3-6	[1]	0.030	0.193	0.027	0.080	0.077	0.045	0.092	0.07
NWA869	L3-6	[2]	0.029	0.189	0.027	0.097	0.069	0.042	0.090	0.04
AÏr	L6	[2]	0.034	0.210	0.032	0.087	0.231	0.055	0.015	0.05

AÏr	L6	[2]		0.030	0.148	0.030	0.142	0.190	0.034	0.013	
AÏr	L6	[2]		0.031	0.178	0.028	0.117	0.202	0.040	0.013	0.01
Kunashak (Slice)	L6	[1]		0.033	0.166	0.023	0.121	0.018	0.042	0.140	2.09
Kunashak (Fragment)	L6	[1]		0.036	0.160	0.029	0.758	0.019	0.042	0.111	2.27
Khohar	L3.6	[2]		0.031	0.113	0.033	0.230	1.989	0.001	0.019	
Kyle	L6	[2]		0.039	0.213	0.024	0.104	0.103	0.056	0.009	0.06
Kyle	L6	[2]		0.034	0.152	0.023	0.083	0.108	0.041	0.008	0.04
Peace River (Fragment)	L6	[1]		0.038	0.185	0.091	0.129	0.327	0.042	0.095	24.83
Fayateville	H4	[2]		0.032	0.147	0.020	0.153	0.527	0.041	0.011	0.27
Pultusk	H5	[2]		0.032	0.149	0.018	0.229	0.191	0.042	0.011	0.07
Pultusk	H5	[2]		0.031	0.131	0.020	0.195	0.163	0.030	0.012	
Forest City	H5	[2]		0.037	0.224	0.023	0.140	0.095	0.063	0.012	0.14
Forest City	H5	[2]		0.037	0.175	0.023	0.083	0.076	0.042	0.012	
Richardton (Fragment)	H5	[1]		0.033	0.154	0.027	0.307	0.347	0.041	0.100	3.68
Carbonaceous											
Ivuna	CI	[1]		0.030	0.117	0.024	0.108	2.691	0.033	0.008	
Ivuna	CI	[1]		0.028	0.117	0.023	0.102	2.676	0.032	0.008	
Tagish Lake	$C2_{ung}$	[2]		0.033	0.204	0.022	0.126	1.582	0.065	0.011	1.47
NWA5958	$C2_{ung}$	[2]		0.033	0.161	0.017	0.173	1.709	0.045	0.058	1.79
NWA5958	$C2_{ung}$	[1]		0.039	0.144	0.023	0.106	1.533	0.042	0.090	
Banten	CM2	[2]		0.035	0.218	0.021	0.151	1.964	0.068	0.011	1.70
Banten	CM2	[2]		0.031	0.139	0.018	0.125	1.674	0.041	0.009	1.25
Murray	CM2	[2]		0.057	0.736	0.082	0.289	3.347	0.858	0.3025	1.70
Murchison (MTF 2005)	CM2	[1]		0.032	0.129	0.021	0.272	1.376	0.036	0.081	154.85
Murchison (Fragment)	CM2	[1]		0.063	0.293	0.033	0.589	1.681	0.048	0.123	121.09
Allende (UCSD 142)	CV3	[1]		0.038	0.158	0.027	0.253	1.286	0.057	0.012	79.04
Allende	CV3	[2]		0.039	0.165	0.026	0.202	1.555	0.052	0.013	0.86
Allende (Literature)	CV3			*0.046*	*0.188*	*0.033*	*0.200*	*1.520*	*0.078*	*0.0174*	
GRA06101	CV3	[2]		0.059	0.382	0.029	0.183	1.040	0.134	0.0130	0.55
Maralinga	$CK4_{an}$	[2]		0.044	0.213	0.028	0.156	0.746	0.121	0.0223	0.60
Maralinga	$CK4_{an}$	[2]		0.040	0.174	0.027	0.150	0.711	0.082	0.0216	0.48
Enstatite											
LON91400	EL6	[2]		0.023	0.189	0.013	0.124	0.134	0.040	0.0048	0.06
Eagle	EL6	[2]		0.023	0.139	0.009	0.186	0.256	0.027	0.0039	0.83
Atlanta	EL6	[2]		0.030	0.269	0.016	0.170	0.595	0.101	0.0118	0.11
Khaipur	EL6	[2]		0.021	0.129	0.014	0.191	0.335	0.030	0.0037	0.09
Khaipur	EL6	[2]		0.022	0.088	0.015	0.162	0.213	0.002	0.0038	
Standards and TPBs											
BHVO-2		[1]	Av.	0.27	4.34	1.13	0.21	1.76	1.24	0.41	86.2
(n = 3)			RSD	3%	3%	2%	6%	4%	5%	3%	1%
BHVO-2		[2]	Av.	0.27	4.36	1.14	0.21	1.60	1.22	0.40	1.0
(n = 4)			RSD	2%	2%	3%	3%	17%	2%	3%	4%
			Rec.	*0.27*	*4.36*	*1.14*	*0.21*	*1.60*	*1.22*	*0.40*	
BCR-2		[1]	Av.	0.45	4.49	0.71	0.42	8.95	5.45	1.51	235.9
(n = 3)			RSD	1%	1%	2%	3%	2%	1%	2%	6%
BCR-2		[2]	Av.	0.48	4.64	0.72	0.41	9.50	5.69	1.57	3.2
(n = 3)			RSD	4%	5%	7%	6%	5%	4%	4%	7%
			Rec.	*0.51*	*4.80*			*11.00*	*6.20*	*1.69*	
BIR-1		[1]	Av.	0.24	0.56	0.04	0.10	2.78	0.03	0.10	38.5
(n = 3)			RSD	4%	4%	4%	87%	2%	1%	5%	4%
			Rec.	*0.26*	*0.60*			*3.00*			
TPB (n = 4)		[1]	Av.	0.00003	0.0012	0.0012	0.070	0.014	0.001	0.004	0.1
TPB (n = 3)		[2]	Av.	0.00003	0.0248	0.0001	0.014	0.007	0.011	0.0001	0.0067

Published data for Allende are from Jarosewich et al. (1987) and Stracke et al., 2012; data for BHVO-1, BCR-2 and BIR-1 are from GeoREM. Allende UCSD 142 was previously reported in Day et al. (2015), with the exception of Ag and Cd composition. TPB = Total Procedural Blank.

[a] [1] Paar bombs used for sample digestion; [2] Teflon beakers used for sample digestion.

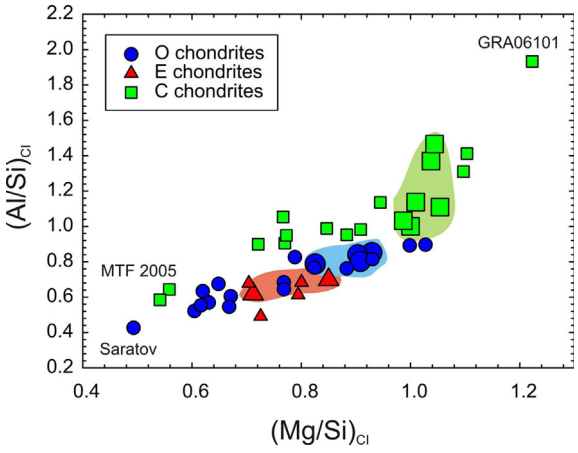

Fig. 5. CI chondrite normalized Mg/Si versus Al/Si for ordinary (O), enstatite (E), and carbonaceous (C) meteorites. Data have been corrected for excess O and are plotted versus averages of chondrite groups (large symbols with surrounding fields) and their normalization, both of which are from (Alexander, 2019a,b).

ple aliquots with and without fusion crust are similar, the fusion crust composition is not considered to be representative of Chelyabinsk's bulk composition. The Olivenza sample shows a strong enrichment in Ba, whereas Th was below detection limits (BDL). The "Low Iron" (L) ordinary chondrite group ranging from L3 to L6 are shown in Fig. 7b. Among these, the NWA869 sample has relative Ba, U and Sr enrichments compared with elements of similar incompatibilities in both aliquots measured. One Saratov aliquot shows a minor enrichment in Ba by a factor of 10 compared to the other sample aliquots. Khohar appears to be a distinct sample given its depletions in Rb, Ba, and more significantly, Th, compared to other samples in the group. Khohar also shows a minor enrichment of Y. Kunashak (L6) samples show enrichments in U and Peace River shows enrichments of Ba, U, and Ta (Fig. 7c). The "High Iron" (H) ordinary chondrite group displays minor enrichments in all incompatible trace elements relative to CI-chondrite Orgueil (Fig. 7d). The Richardton - fragment (H5), exhibits enrichments in U and Ti compared to the rest of the group. One of the Forest City (H5) aliquots shows a minor enrichment in Zr and Hf.

Incompatible trace element patterns for Enstatite chondrites are shown in Fig. 8. Enstatite chondrites from this study show depletions in most incompatible trace elements compared to CI-chondrite Orgueil. However, for the sample Atlanta, there are slight enrichments in Th, Zr and Hf. Khaipur shows the most significant depletions in

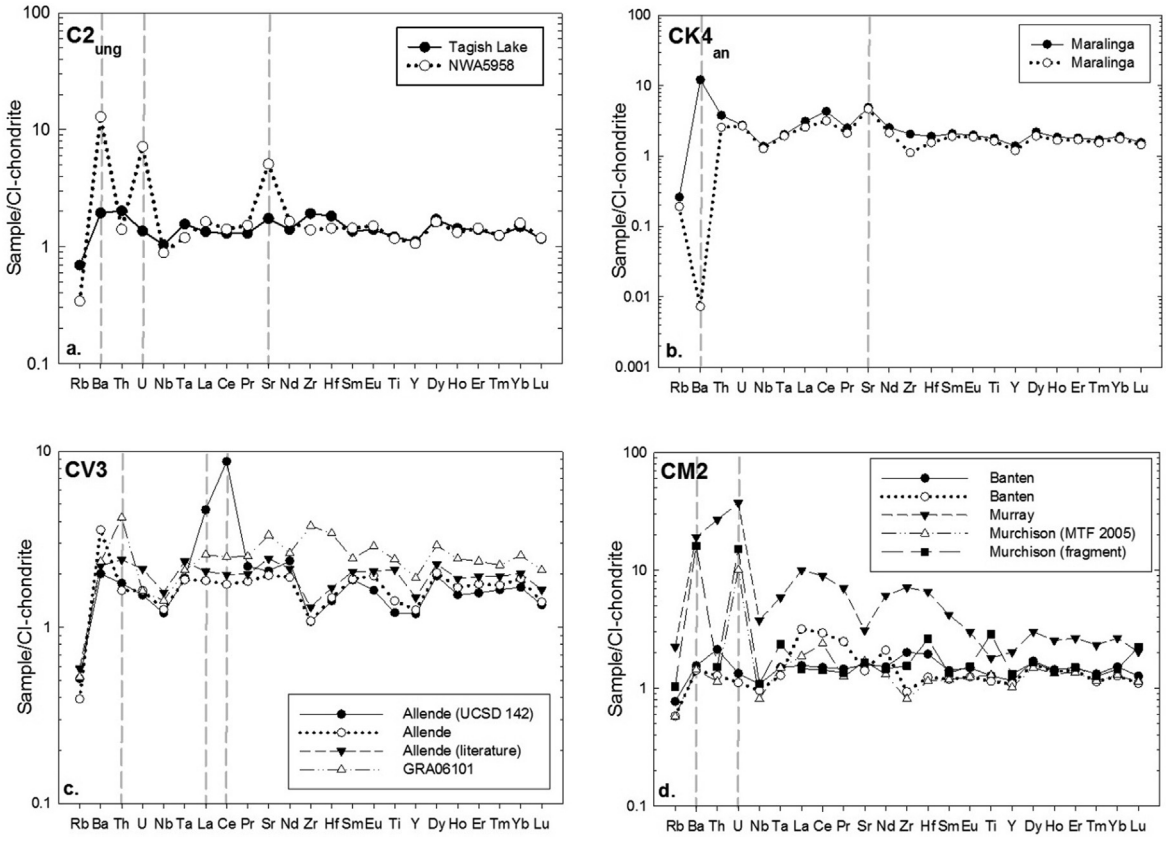

Fig. 6. Incompatible trace element compositions for carbonaceous chondrites measured in this study. (a). Incompatible trace elements in $C2_{ung}$ chondrites. (b). Incompatible trace elements in $CK4_{an}$ chondrites. (c). Incompatible trace elements in CV3 chondrites. (d). Incompatible trace elements in CM2 chondrites. Elements are ordered from most incompatible (Rb) on the left to least incompatible (Lu) on the right. All samples are normalized to CI chondrite values obtained for Orgueil from Friedrich et al., (2002), with Ta normalization from Barrat et al., (2012).

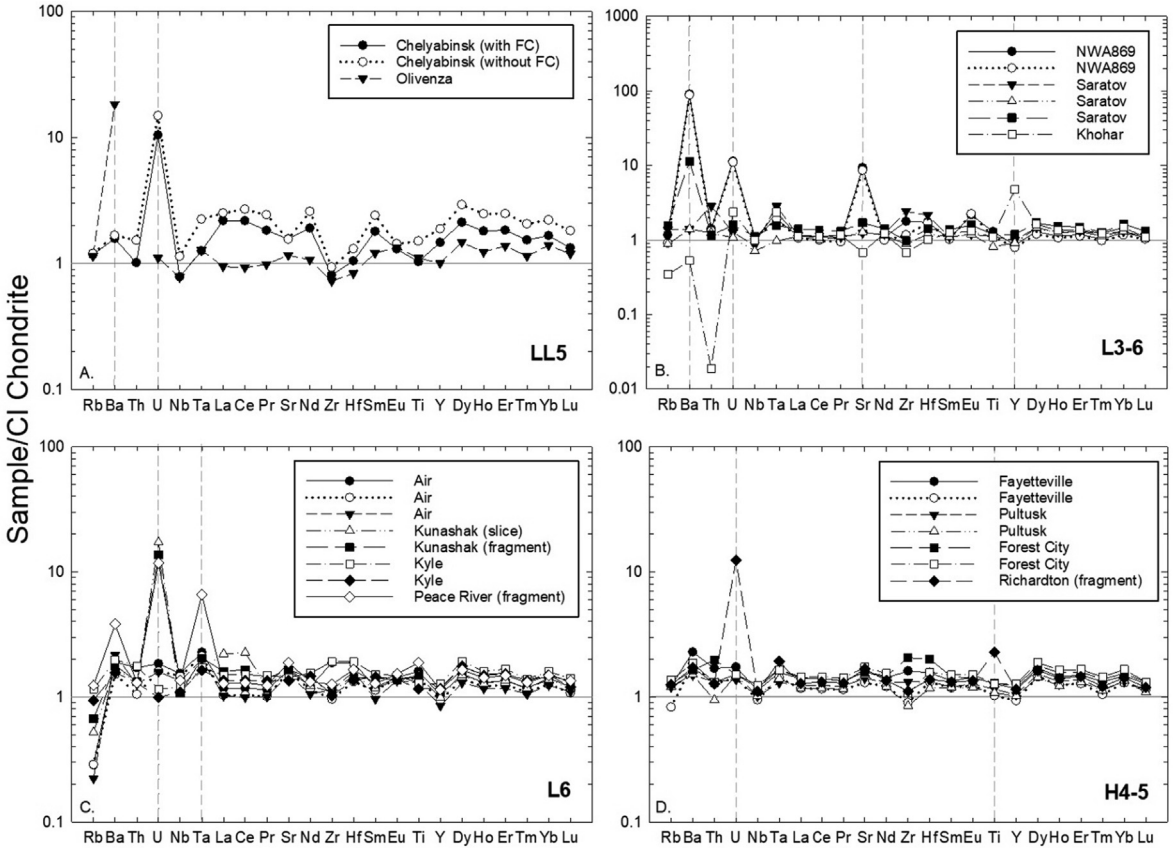

Fig. 7. Incompatible trace elements in ordinary chondrites from this study. Plots are separated into "Low metal/Low Iron (LL5)" (A.), "Low Iron (L3-6 and L6)" (B. and C.) and "High Iron (H4-5)" ordinary chondrites (D.). Normalization as in Fig. 6.

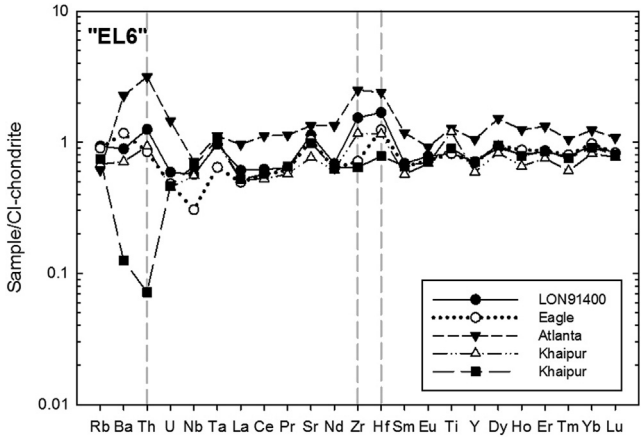

Fig. 8. Incompatible trace elements in "Low Enstatite" enstatite chondrites from this study. Normalization as in Fig. 6.

incompatible trace elements out of all the samples measured, although it does have a slight enrichment in Zr and Hf, following the pattern of the other samples in the group.

It should be noted that, for all chondrite classes, small but significant variations are found in Zr and Hf, relative to the normalizing CI chondrite value from Barrat et al., (2012). These variations could be significant from the perspective of the distribution of Zr and Hf in chondrites, or they may reflect inefficient digestion of phases that contain Zr and Hf (zircon and Zr-rich phases) in prior studies, which we return to in the discussion.

4.4. Rubidium-strontium isotope systematics

New ^{87}Rb-^{87}Sr systematics for the meteorites examined in this study are given in Fig. 9 and are reported in Table 5.

Table 5
Rubidium-strontium isotope data for chondrites.

Sample	Type	Mass (g)	Rb (ppm)	Sr (ppm)	$^{87}Rb/^{86}Sr$	*2SD*	$^{87}Sr/^{86}Sr$	*2SE*
Carbonaceous								
NWA5958	$C2_{ung}$	0.00554	0.77	34.83	0.0641	*0.0038*	0.712648	*0.000004*
Murray	CM2	0.00542	5.05	21.01	0.6954	*0.0417*	0.722684	*0.000067*
Banten	CM2	0.04408	1.31	9.01	0.4201	*0.0252*	0.714491	*0.000053*
(rerun)		0.04408	1.31	9.01	0.4201	*0.0252*	0.729962	*0.000007*
		0.02045	1.74	10.33	0.4881	*0.0293*	0.729901	*0.000012*
Allende	CV3	0.04892	0.89	12.62	0.2034	*0.0122*	0.715343	*0.000003*
GRA06101	CV3	0.00492	1.18	23.00	0.1490	*0.0089*	0.712423	*0.000040*
Maralinga	$CK4_{an}$	0.04925	0.43	29.79	0.0419	*0.0025*	0.708947	*0.000003*
		0.02014	0.59	31.80	0.0536	*0.0032*	0.708780	*0.000004*
Ordinary								
Olivenza	LL5	0.00540	2.60	7.47	1.0079	*0.0605*	0.755786	*0.000220*
NWA869	L3-6	0.05016	2.05	55.22	0.1072	*0.0064*	0.716653	*0.000002*
		0.02002	2.65	61.31	0.1250	*0.0075*	0.716733	*0.000005*
Khohar	L3-6	0.00839	4.38	8.47	1.4972	*0.0898*	0.790811	*0.000012*
Saratov	L4	0.04268	3.56	10.92	0.9440	*0.0566*	0.762814	*0.000004*
		0.05008	2.00	8.19	0.7060	*0.0424*	0.762848	*0.000004*
		0.00570	3.12	9.09	0.9944	*0.0597*	0.766298	*0.000016*
Kyle	L6	0.05500	2.12	8.63	0.7101	*0.0426*	0.753639	*0.000003*
		0.02058	2.60	9.51	0.7906	*0.0474*	0.753714	*0.000007*
Aïr	L6	0.04603	0.65	10.14	0.1858	*0.0111*	0.736288	*0.000003*
		0.04924	0.51	9.58	0.1525	*0.0091*	0.736056	*0.000005*
		0.02044	0.65	10.75	0.1737	*0.0104*	0.735853	*0.000005*
Fayettville	H4	0.04540	1.87	8.32	0.6521	*0.0391*	0.750328	*0.000002*
		0.02022	2.75	10.36	0.7690	*0.0461*	0.749258	*0.000012*
Forest City	H5	0.04493	3.08	11.04	0.8080	*0.0485*	0.753416	*0.000003*
(AMNH2421)		0.02075	2.88	10.55	0.7890	*0.0473*	0.752639	*0.000006*
Pultusk	H5	0.04456	2.73	9.56	0.8273	*0.0496*	0.753418	*0.000003*
		0.02081	2.70	9.22	0.8469	*0.0508*	0.752152	*0.000007*
Enstatite								
Khairpur	EL6	0.01329	1.69	6.30	0.7764	*0.0466*	0.746725	*0.000004*
		0.00549	1.54	6.22	0.7147	*0.0429*	0.748595	*0.000043*
LON91400	EL6	0.02020	2.11	7.61	0.8013	*0.0481*	0.754406	*0.000017*
Eagle	EL6	0.00525	2.03	8.03	0.7314	*0.0439*	0.736750	*0.000087*
Atlanta	EL6	0.00518	1.38	9.81	0.4067	*0.0244*	0.724527	*0.000008*

Carbonaceous chondrite $^{87}Rb/^{86}Sr$ and $^{87}Sr/^{86}Sr$ ratios range between 0.042 to 0.695 and 0.708824 to 0.730008, respectively. Data from this study in both CM2 and CV3 groupings agree well with previous studies (Kaushal and Wetherill, 1970; Murthy and Compston, 1965; Mittlefehldt and Wetherill, 1979), although the fragment of Murray (CM2) that we measured has a higher $^{87}Rb/^{86}Sr$ ratio for a given $^{87}Sr/^{86}Sr$ composition. Ordinary chondrites show $^{87}Rb/^{86}Sr$ and $^{87}Sr/^{86}Sr$ ratios ranging between 0.107 to 1.50 and 0.716698 to 0.790860 respectively. In general, H and L chondrites measured in this study agree well with previous studies (Minster and Allegre, 1981; Minster and Allegre, 1979a,b). Khohar (L3-6) has a $^{87}Rb/^{86}Sr$ ratio that is two-times the average value for other L chondrites. Northwest Africa 869 and Saratov have measurements of $^{87}Sr/^{86}Sr$ that are higher than most other L chondrites, pulling them away from the trendline in Fig. 9B. Finally, the Olivenza $^{87}Rb/^{86}Sr$ ratio value from this study (1.0079) differs from previous measurements (0.7790: Minster and Allegre, 1981); this difference is likely due to the small sample size used in this study and non-representativeness. Enstatite chondrites measured in this study have $^{87}Rb/^{86}Sr$ and $^{87}Sr/^{86}Sr$ ratios ranging between 0.407 to 0.801 and 0.724572 to 0.754453. Measurements done on the EL6 chondrites of this study are similar to those from previous studies (Minster et al., 1979; Gopalan and Wetherill, 1970), although Eagle (EL6) falls slightly off the trendline (Fig. 9C).

4.5. Oxygen isotopes

Oxygen isotopes were measured for seven chondrites from the studied sample suite and are reported in Table 6 and shown in Fig. 10. Multiple measurements were run on all samples except NWA 869. Comparisons are made to the terrestrial fractionation line (TFL), which has a slope of 0.5305 (Criss and Farquhar, 2008). Ordinary chondrites from this study fall within the LL, L and H grouping from previous studies (Yurimoto et al., 2008; Clayton and Mayeda, 1999; Clayton et al., 1984). Two results from Chelyabinsk (LL5) fall outside of the LL grouping but within the H grouping. These variable results for Chelyabinsk

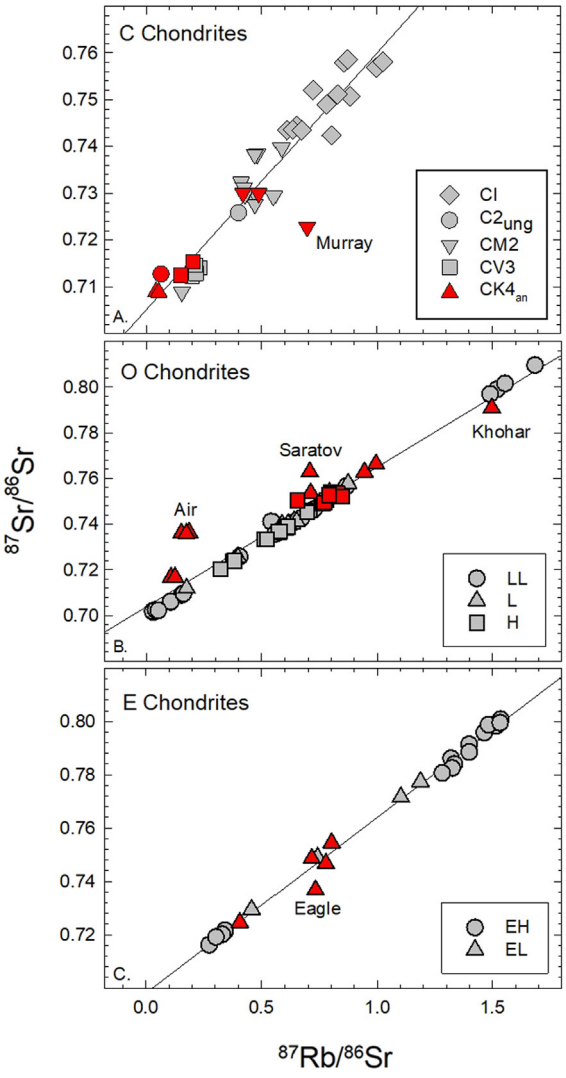

Fig. 9. $^{87}Rb/^{86}Sr$ versus $^{87}Sr/^{86}Sr$ isotopic ratios for the carbonaceous, ordinary and enstatite chondritic meteorites examined in this study versus literature values for the same groups. Symbols in red are from this study, symbols in gray are from previous studies. Regression lines calculated from all data are included in each plot. (Carbonaceous sources: Kaushal and Wetherill (1970); Murthy and Compston (1965); Mittlefehldt and Wetherill (1979); Ordinary sources: Minster and Allegre (1981); Minster and Allegre (1979a,b); Enstatite sources: Minster and Allegre (1982); Gopalan and Wetherill (1970)).

may be evidence of H-chondrite nuggets or remelted material. Carbonaceous chondrites from this study fall within the groupings represented in previous studies (Brown et al., 2013). Among all the samples measured in this study, Allende shows the most variation in oxygen isotopic composition.

To examine O isotope relationships, regression lines were fitted to the data. The regression line for ordinary chondrites measured in previous studies (OC_1) differs to that of the ordinary chondrites measured in this study (OC_2) (Yurimoto et al., 2008, Clayton and Mayeda, 1999). From this study, Peace River (L6), NWA 869 (L3-6) and Chelyabinsk (LL5) all fall along both regression lines (OC_1, OC_2), however, Richardton (H5) and Kunashak (L6) show a slight depletion in both $\delta^{18}O$ and $\delta^{17}O$ relative to the measurements from Yurimoto et al., 2008, offsetting the regression lines of the two separate sample sets. The data collected from this study on the carbonaceous chondrites, Allende and Murchison, falls along the regression line from data collected in Yurimoto et al., 2008. Measurements on Murchison, however, showed variable results between the two studies; the $\delta^{18}O = 1.41$ and $\delta^{17}O = -3.52$ from this study and $\delta^{18}O = 7.3$ and $\delta^{17}O = 1.196$ from Yurimoto et al., 2008 giving a $\Delta^{17}O$ value different by a factor of ~2 (Table 6). These results are consistent with the aliquot sampling approach in this study, likely reflecting oxygen heterogeneities resulting from heterogeneous materials (i.e., chondrules and CAIs) forming at different times and experiencing variable conditions in the solar nebula and alteration events on their parent bodies (Krot et al., 1998).

4.6. Highly siderophile element abundances of chondrites

New HSE abundance and Re-Os isotope data are reported in Table 7, with all similar and previously published data (until 2021) for chondrites given in Table S1 for comparison. The new dataset includes six, four and three individual analyses of powders of Allende (CV3), Chelyabinsk (LL5) and Tagish Lake (C2), respectively; Fig. 11 presents data from this and prior studies for Tagish Lake and Allende. Tagish Lake has previously been examined for HSE abundances and Os isotopes by Brandon et al., (2005a) and Allende has been measured for HSE abundances by over half-a-dozen studies using a range of analytical methods. The new data for Tagish Lake are similar to the highest concentration measurements by Brandon et al., (2005a), but measurements from this study show systematically higher Ir and Pt. Excellent reproducibility is found in the aliquots of Allende measured in this study versus published literature (Horan et al., 2003; Fischer-Gödde et al., 2010; Walker et al., 2002; Brandon et al., 2005a), with the exception of one aliquot that had higher Re and Os contents (Fig. 11). In general, HSE absolute abundances within individual aliquots of samples can vary due to metal inclusions, calcium aluminum inclusions (CAIs) or uneven distributions of various mineral phases. However, the correspondence between data from this study and published values for chondrites (Horan et al., 2003; Fischer-Gödde et al., 2010; Morgan et al., 1985; McDonald et al., 2001; Walker et al., 2002; van Acken et al., 2011; Goderis et al., 2017) indicates that, in general, homogenization of powdered samples leads to similar relative and absolute HSE abundances. There are a few exceptions, such as, where metal rich components were preferentially measured in CB chondrites (e.g., Gujba, this study; Hammafah al Hamra (Hah) 237 (CB_b), Walker et al., 2002).

The new HSE abundance data for all measured chondrites are presented with published data (Horan et al., 2003; Fischer-Gödde et al., 2010; Walker et al., 2002; Brandon et al., 2005a; van Acken et al., 2011; Goderis et al., 2017) (Table S1) in Fig. 12. The abundance data from

Table 6
Oxygen isotope compositions of selected chondrite meteorites.

Sample	Type	$\delta^{18}O$	2SD	$\delta^{17}O$	2SD	$\Delta^{17}O$	2SD	*n*
Ordinary								
Chelyabinsk	LL5	4.43	0.01	3.57	0.03	1.25		
		2.66	0.03	2.79	0.04	1.40		
		2.76	0.01	2.70	0.03	1.26		
						1.30	***0.16***	***3***
Chelyabinsk (FC)	LL5	4.59	0.03	3.65	0.04	1.25		
		4.57	0.02	3.72	0.06	1.33		
		4.63	0.02	3.65	0.03	1.22		
						1.27	***0.11***	***3***
Kunashak	L6	4.15	0.02	3.45	0.12	1.28		
		4.12	0.03	3.29	0.06	1.13		
		4.01	0.02	3.29	0.02	1.19		
		4.02	0.02	3.26	0.01	1.15		
						1.19	***0.13***	***4***
Peace River	L6	4.32	0.02	3.78	0.17	1.52		
		4.29	0.01	3.50	0.02	1.25		
		4.15	0.04	3.60	0.07	1.43		
		4.15	0.02	3.42	0.07	1.24		
						1.36	***0.28***	***4***
NWA 869	L3-6	4.56	0.01	3.80	0.05	1.42		*1*
Richardton	H5	4.40	0.01	3.30	0.04	1.00		
		4.10	0.02	2.96	0.03	0.81		
		4.38	0.03	2.87	0.03	0.58		
		4.04	0.01	3.11	0.04	1.00		
						0.85	***0.39***	***4***
Carbonaceous								
Murchison	CM2	1.92	0.05	−3.30	0.07	−4.31		
		1.87	0.03	−3.63	0.05	−4.61		
						−4.46	***0.43***	***2***
Allende	CV3	−1.95	0.02	−5.49	0.02	−4.47		
		−3.04	0.04	−5.78	0.02	−4.18		
		−2.98	0.03	−5.85	0.05	−4.29		
						−4.31	***0.29***	***2***

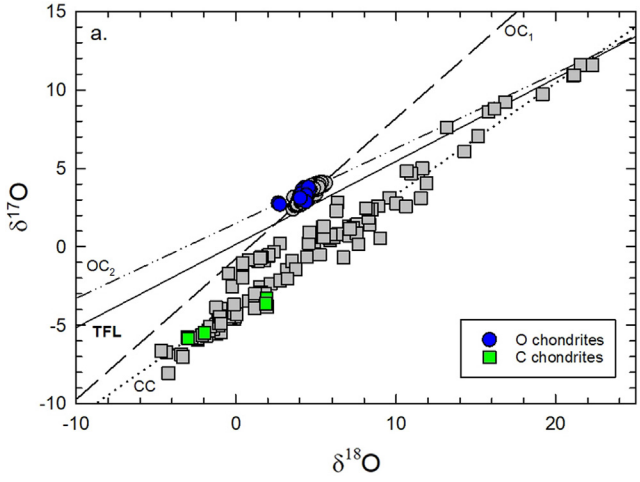

Fig. 10. $\delta^{18}O$ versus $\delta^{17}O$ in per mil (‰). OC_1-ordinary chondrite regression line using data from previous studies (references below). OC_2 – ordinary chondrite regression line for data from this study. CC-carbonaceous chondrite regression line. TFL-Terrestrial Fractionation Line (slope: 0.5241). All grey symbols are from Yurimoto et al., 2008; Clayton and Mayeda, (1999) and Clayton et al., (1984).

Table 7
Rhenium-osmium isotope and highly-siderophile element abundances (ppb) for Chelyabinsk and other chondrite meteorites.

Sample	Type	Mass (g)	Os	Ir	Ru	Pt	Pd	Re	$^{187}Re/^{188}Os$	2SD	$^{187}Os/^{188}Os$	2SD	$^{187}Os/^{188}Os_i$	2SD	ΔOs[1]
Ordinary															
Chelyabinsk	LL5	0.0328	655.4	614.5	961.9	1344.6	1237.5	65.9	0.485	0.033	0.13269	0.00013	0.0944	0.0038	−8
		0.0322	351.7	343.2	463.7	633.5	398.0	28.0	0.383	0.018	0.12457	0.00017	0.0943	0.0021	−9
		0.049	503.7	441.3	715.4	816.7	504.0	39.5	0.378	0.025	0.12526	0.00008	0.0954	0.0029	2
Chelyabinsk (with FC)	LL5	0.094	445.9	445.9	727.4	907.9	588.4	38.7	0.418	0.022	0.12835	0.00007	0.0953	0.0026	2
Saratov	L4	0.027	647.6	632.3	954.4	1507.2	786.8	66.1	0.493	0.032	0.13312	0.00012	0.0942	0.0037	−10
NWA869	L3-6	0.028	551.8	548.1	748.4	990.4	610.6	101.8	0.889	0.028	0.12672	0.00011	0.0564	0.0034	−386
Khohar	L3-6	0.007	743.0	751.8	1097.9	1479.5	874.1	66.6	0.432	0.037	0.12844	0.00013	0.0943	0.0042	−9
Aïr	L6	0.030	730.7	676.4	1049.0	1467.5	849.0	70.9	0.468	0.037	0.12997	0.00007	0.0930	0.0042	−22
Kunashak	L6	0.100	440.6	414.7	693.3	925.8	447.1	37.0	0.404	0.022	0.12567	0.00007	0.0937	0.0026	−15
Kunashak	L6	0.100	499.6	499.0	856.0	1160	546.6	40.3	0.388	0.025	0.12572	0.00006	0.0950	0.0029	−1
Peace River	L6	0.097	570.4	507.6	926.9	1221	494.2	49.5	0.418	0.029	0.12836	0.00009	0.0953	0.0033	2
Kyle	L6	0.095	451.2	438.9	620.6	835.4	531.2	43.0	0.459	0.023	0.12749	0.00009	0.0912	0.0026	−40
Fayetteville	H4	0.094	763.4	726.3	1062.8	1459	809.2	66.0	0.417	0.038	0.12880	0.00003	0.0958	0.0043	7
Pultusk	H5	0.029	1070	1045	1483	2082	1188	100.8	0.455	0.053	0.13177	0.00013	0.0958	0.0060	7
Forest City	H5	0.030	842.7	1023	808.3	1489	770.8	74.1	0.424	0.042	0.12765	0.00013	0.0942	0.0048	−10
Richardton	H5	0.055	1114	1010	1770	2180	958.7	105.1	0.455	0.056	0.12829	0.00009	0.0923	0.0063	−28
Carbonaceous															
Ivuna	CI	0.002	434.0	453.1	625.0	774.4	568.8	40.5	0.450	0.022	0.12632	0.00012	0.0907	0.0025	−44
Orgueil	CI	0.007	472.6	500.9	689.2	940.2	637.5	40.3	0.411	0.024	0.12654	0.00011	0.0940	0.0027	−11
Tagish Lake	C2-ugr	0.030	548.9	572.4	845.3	1083	624.5	41.7	0.366	0.027	0.12630	0.00012	0.0974	0.0031	22
		0.029	533.6	571.5	774.5	1007	622.3	43.0	0.388	0.027	0.12669	0.00009	0.0960	0.0031	8
		0.131	566.1	578.2	837.1	1107	592.6	46.9	0.400	0.028	0.12803	0.00017	0.0964	0.0032	13
NWA 5958	C2	0.025	482.7	575.8	703.8	510.2	540.1	18.8	0.188	0.024	0.12985	0.00014	0.1150	0.0027	198
Gujba	CBa	0.024	3337	3059	5040	6648	3363	295.0	0.426	0.167	0.12566	0.00014	0.0920	0.0187	–32
Banten	CM2	0.092	616.8	615.0	845.5	1063	654.2	55.2	0.432	0.031	0.12697	0.00007	0.0928	0.0035	–23
Cold Bokkeveld	CM2	0.009	556.0	572.0	829.7	1117	685.2	45.8	0.397	0.028	0.12549	0.00029	0.0941	0.0032	−10
Murray	CM2	0.120	525.6	553.3	773.7	1024	615.9	42.9	0.393	0.026	0.12691	0.00036	0.0958	0.0030	7
Murchison MTF	CM2	0.101	557.9	570.9	990.1	1266	600.1	48.1	0.416	0.028	0.12649	0.00007	0.0936	0.0032	−15
Murchison SIGL	CM2	0.119	572.4	525.2	847.1	1135	537.8	85.8	0.722	0.029	0.12484	0.00006	0.0677	0.0034	−274
Allende	CV3	0.101	737.6	717.7	1031	1503	637.7	64.3	0.420	0.037	0.12586	0.00007	0.0926	0.0042	−25
		0.101	666.4	657.4	994.9	1385	627.2	55.4	0.400	0.033	0.12588	0.00007	0.0942	0.0038	−9
		0.100	711.3	723.6	1033	1378	758.4	63.5	0.430	0.036	0.12643	0.00014	0.0924	0.0040	−27
		0.100	871.0	698.0	1017	1344	738.7	75.7	0.419	0.044	0.12540	0.00017	0.0923	0.0049	−29
		0.101	701.4	663.2	1026	1354	739.3	60.3	0.414	0.035	0.12631	0.00033	0.0935	0.0040	−16
		0.034	764.3	762.7	1091	1447	593.3	64.3	0.406	0.038	0.12659	0.00009	0.0945	0.0043	−7
Graves Nunataks 06101	CV3	0.018	847.8	937.6	1322	1681	805.6	74.6	0.424	0.042	0.12795	0.00009	0.0944	0.0048	−8
NWA 4502	CV3	0.030	880.9	941.8	1215	1487	888.7	47.5	0.260	0.044	0.12565	0.00016	0.1051	0.0049	99
Maralinga	CK4-an	0.031	692.1	710.4	920.4	1576	98.7	21.8	0.152	0.035	0.11351	0.00007	0.1015	0.0039	63
Enstatite															
Eagle	EL6	0.030	940.3	904.0	1131	1551	1229	75.9	0.389	0.047	0.12522	0.00010	0.0945	0.0053	−7
Atlanta	EL6	0.030	663.9	653.9	930.4	1254	708.3	64.6	0.469	0.033	0.12767	0.00010	0.0906	0.0038	−46

LON91400	EL6	0.030	788.1	765.7	1060	1482	921.2	70.9	0.434	0.039	0.12782	0.00011	0.0935	0.0045	−16
Khairpur	EL6	0.010	1257	1178	1660	2323	1389	110.7	0.424	0.063	0.12808	0.00012	0.0945	0.0071	−6
Khairpur	EL6	0.010	1257	1660	1178	2323	1389	110.7	0.424	0.063	0.12808	0.00012	0.0945	0.0071	−6
Literature data[2]															
Allende[a]			729	684	1007	1357	674	60.5	0.393		0.12595				−3
Allende[b]			763	700	1140	1379	786	61.2	0.386		0.12638				7
Allende[c]			785	720	1118	1421	682	63.5	0.390		0.12596				0
Allende[d]			758	712	1016	1348	674	60.9	0.387		0.12615				4
Allende[e]			746	730	843	1290		60.2							
Allende[f]				694	1058	1395	598								
Allende[g]			833	776			705	68.4							
Allende[h]				740											
Murchison[d]			580	558	741	1043	629	46.0	0.393		0.12526				−10
Murchison[a]			572	569	843	1127	151	46.7	0.382		0.12609				7

[1] ΔOs (after Fischer-Gödde et al. 2010) refers to the combined deviation in the determined $^{187}Os/^{188}Os$ and $^{187}Re/^{188}Os$ for a given chondrite sample from the IIIA iron meteorite reference isochron, $\Delta Os = 10^4 (^{187}Os/^{188}Os_{chondrite} - (0.09524 + 0.07887 \times {}^{187}Re/^{188}Os_{chondrite}))$. $^{187}Os/^{188}Os_{chondrite}$ and $^{187}Re/^{188}Os_{chondrite}$ are the values determined for chondrites, 0.09524 is the initial $^{187}Os/^{188}Os$ and 0.07887 is the slope of the IIIA iron meteorite isochron (Smoliar et al., 1996).

[2] a = [ID CT/HPA] Fischer-Gödde et al. (2010); b = [ID CT] Becker et al. (2006); c = [ID CT] Brandon et al. (2005a,b); d = [ID CT] Walker et al. (2002) and Horan et al. (2003); e = [Spark source mass spectrometry] Jochum (1996); f = [NiS] Tagle and Berlin (2008); g = [RNAA] Takahashi et al., 1978; h = [Recommended Values] Jarosewich et al. (1987); i = [Average NAA] Swindle et al. (1998).

this study are broadly consistent with the published data, expanding the range of absolute abundances measured in the groups. Enstatite chondrites show the greatest spread of HSE abundances (~0.2 to ~2.8 × CI-chondrite) compared to carbonaceous or ordinary chondrites. The Richardton H5 chondrite shows a notable relative enrichment in Ru compared to CI chondrites. Most HSE abundances measured in the various chondrite classes are higher relative to CI-chondrite Orgueil, to which their abundances are normalized (based on compiled data from Day et al., 2016b). This deviation is likely to be due to dilution effects due to the presence of higher volatile components within CI-chondrites (Day et al., 2016b), from potential modification by later impact processes (Norman and Mittlefehldt, 2001), and possibly due to preferential sampling of HSE-rich components in the meteorites from the limited aliquot sizes prepared.

As expected, absolute HSE abundances in ordinary chondrites increase with metal abundances, where LL < L < H. Similar to previous studies, data from this study on ordinary chondrites show no correlation between the petrologic type and HSE abundance (Fig. 13B.), suggesting that thermal metamorphism has no control on HSE abundances in the parent bodies of ordinary chondrites (Fischer-Gödde et al., 2010; Kallemeyn et al., 1989; Day et al., 2016b). Carbonaceous chondrites show increasing HSE abundances between the groups in the order CI < CM2 < CV3. Maralinga ($CK4_{an}$) has a significant relative depletion of Pd and NWA 5958 has a depletion in Pt and an enrichment in Pd, relative to CI chondrite (Fig. 12B.). In carbonaceous chondrites, there is a trend for both Os and Pd in association with petrologic type (Fig. 12), where Os shows an increasing abundance relative to increasing petrologic grade, while a similar, but weaker, correlation is observed for Pd. Generally, most carbonaceous chondrites show a minor depletion of Pd relative to the other HSE and have CI-like HSE abundance patterns, excluding the few mentioned above. Gujba (CB_a) has been excluded from figures due to the high HSE content measured for this sample aliquot. The high HSE content is caused by the high metal content and, in this sense, is like Re and Os contents previously reported for CB_b Hah 237 (Walker et al., 2002).

Four enstatite chondrites were measured for HSE abundances in this study, all of which are from the EL group petrologic type 6. Khairpur shows the highest HSE abundances, most notably in its Re abundance (Fig. 12C.). Eagle, Atlanta and LON91400 have similar HSE abundances to enstatite chondrites measured in previous studies (Horan et al., 2003; Fischer-Gödde et al., 2010), although Eagle is comparatively enriched in Ir and Pd. Excluding Khairpur, the enstatite chondrites show a limited spread in HSE abundance. Similar to the ordinary chondrites, the enstatite chondrites do not have strong trends associated with petrologic type (Fig. 13C); it is important to note, however, that the amount of enstatite samples available to measure is far less than carbonaceous or ordinary chondrites. When all chondrites are plotted for both Re and Pd abundances relative to petrologic grade, the variability in concentrations of these elements expands with increasing petrologic type (Fig. 13D).

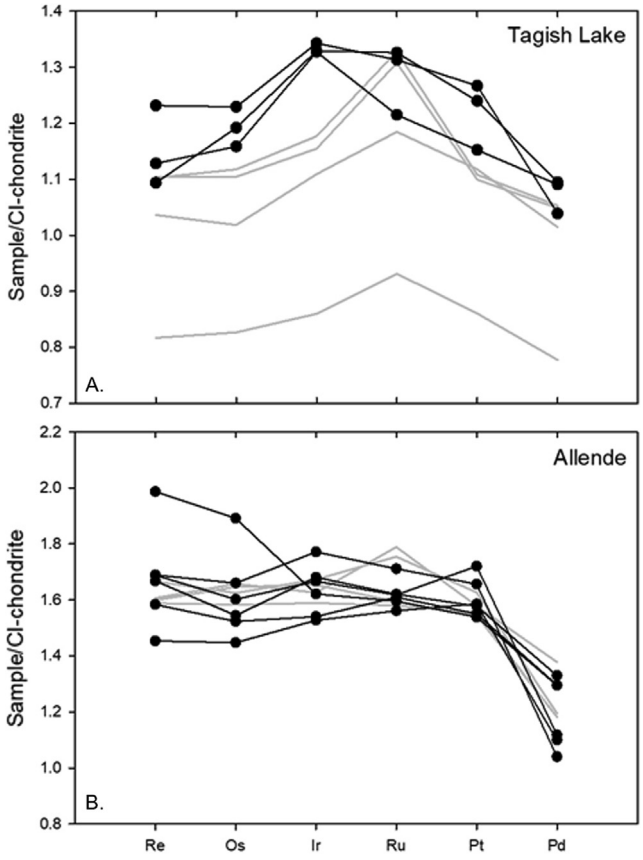

Fig. 11. Linear CI-chondrite normalized HSE patterns for duplicate measurements of Tagish Lake (A.) and Allende (B.) versus analyses from prior studies. Grey lines are measurements from Brandon et al., (2005a); Fischer-Gödde et al., (2010); Becker et al., (2006) and Walker et al., (2002). All samples are normalized to CI-chondrite Orgueil from the compilation in Day et al., (2016b).

Taking the average of the HSE contents for all published chondrites, with the exception of Gujba (CBa), yields the following HSE abundances for ordinary chondrites (n = 41): 599 ng g^{-1} Ir, 902 ng g^{-1} Ru, 1322 ng g^{-1}Pt, 696 ng g^{-1} Pd, with a total of 36% variation in HSE abundances (1 standard deviation); carbonaceous chondrites (n = 89): 646 ng g^{-1} Ir, 946 ng g^{-1} Ru, 1230 ng g^{-1}Pt, 686 ng g^{-1} Pd, with a total of 13% variation in HSE abundances (excluding Hah237 – Walker et al., 2002); enstatite chondrites (n = 50): 564 ng g^{-1} Ir, 897 ng g^{-1} Ru, 1152 ng g^{-1}Pt, 838 ng g^{-1} Pd, with a total of 28% variation in HSE abundances. These average Ir, Ru, Pt and Pd contents and the total variability in HSE abundances indicates that ordinary, carbonaceous and enstatite chondrite reservoirs had identical initial HSE abundances, within uncertainties, consistent with prior work (e.g., Horan et al., 2003; Fischer-Gödde et al., 2010).

4.7. Rhenium-osmium isotope systematics

Data obtained for Re and Os abundances, $^{187}Re/^{188}Os$ and $^{187}Os/^{188}Os$, including calculated $^{187}Os/^{188}Os_i$ at 4568 Ma (assumed time of Solar System formation) are listed in Table 7. In this study, concentrations for Re spanned from 18.8 ng g^{-1} to 295 ng g^{-1} and concentrations of Os spanned from 351 ng g^{-1} to 3337 ng g^{-1}. Aliquots of Chelyabinsk (LL5) and NWA 5958 (C2) had the lowest Os and Re respectively, whereas Gujba (CBa) was the highest for both Re and Os concentrations. As noted previously, it is likely that the reason for Gujba's anomalously high concentrations of Re, Os and other HSE is due to incorporation of metal fractions in the measured sample. As shown by prior studies (Walker et al., 2002), ordinary chondrites tend to have the highest concentrations of Re and Os, most likely due to the greater proportions of metal within sample aliquots (Fig. 14). While carbonaceous chondrites do not vary as greatly in Os concentrations as ordinary or enstatite chondrites, they do have a tendency towards greater offset in Re concentrations and so elevated Re/Os, with respect to ordinary or enstatite chondrites.

Ratios of $^{187}Re/^{188}Os$ versus $^{187}Os/^{188}Os$ for most samples in this study lie along the 4.568 Ga iron meteorite isochron, as has also been observed for chondrite classes previously (Fig. 15; Walker et al., 2002; Brandon et al., 2005a; Fischer-Gödde et al., 2010; van Acken et al., 2011; Goderis et al., 2017). Samples with low Re/Os (NWA 5958, NWA 4502, Maralinga) and high Re/Os (NWA 869, Murchison (SIGL) lie to the left and the right of the isochron, respectively, strongly implicating recent disturbance (Fig. 15). For ordinary chondrites in this study, the $^{187}Re/^{188}Os$ ratios span from 0.378 (Chelyabinsk LL5) to 0.889 (NWA869 L3-6). Excluding NWA869, the range for

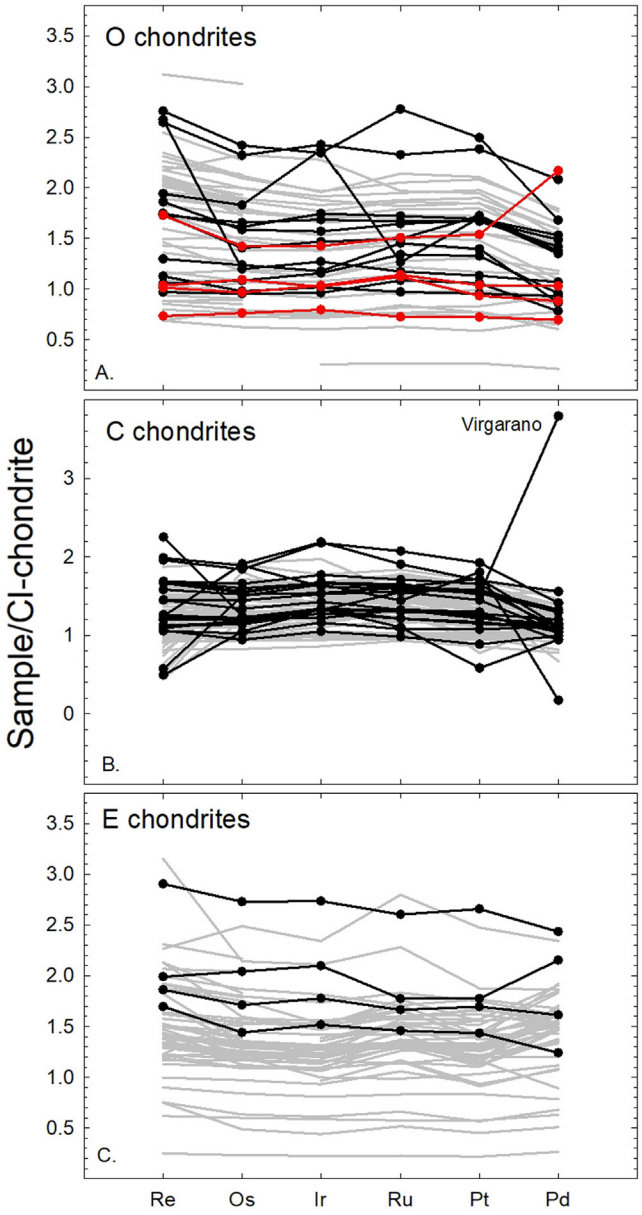

Fig. 12. CI-chondrite normalized HSE abundance patterns between chondrite classes (note Y-axis is as a linear scale). Data from this study (excluding Gujba) are in black, with Chelyabinsk aliquots in red; data from Horan et al., (2003); Fischer-Gödde et al., (2010); Walker et al., (2002); Brandon et al., (2005a); van Acken et al., (2011); Goderis et al., (2017) are in grey. Normalization scheme is the same as for Fig. 11.

ordinary chondrites tapers to 0.378–0.493, with an average of 0.434 ± 0.068 (n = 59, 1 st. dev.), close to the average ratio from Walker et al., (2002) of 0.422 ± 0.025. Carbonaceous chondrites exhibit a range of $^{187}Re/^{188}Os$ ratios, from 0.152 (Maralinga CK4-an) to 0.722 (Murchison CM2); excluding NWA 4502 (0.260), and NWA 5958 (0.188), the range from carbonaceous chondrites narrows to 0.366–0.450, with an average of 0.3965 ± 0.0573 (n = 72, 1 st. dev.). For comparison, the average for carbonaceous chondrites in Walker et al., 2002 was 0.389 ± 0.021. The enstatite chondrites show a range from $^{187}Re/^{188}Os$ = 0.389 Eagle (EL6) to 0.469 Atlanta (EL6), with an average of 0.427 ± 0.020 (n = 39, 1 st. dev.); Walker et al., (2002) showed an average of 0.421 ± 0.013 for enstatite chondrites. In general, the measurements from this sample set correlate closely to those of Walker et al., (2002) but expand upon it.

For carbonaceous chondrites, the $^{187}Os/^{188}Os$ ratios range from 0.10929 to 0.13032, with an average of 0.1252 4 ± 0.0035 (n = 83, 1 st. dev.); for ordinary the range of $^{187}Os/^{188}Os$ ratios is 0.12526 to 0.13312, with an average of 0.1284 ± 0.0021 (n = 59, 1 st. dev.) and for enstatite, $^{187}Os/^{188}Os$ ratios range from 0.12520 to 0.13029 with an average of 0.1281 ± 0.0009 (n = 57, 1 st. dev.). The ranges

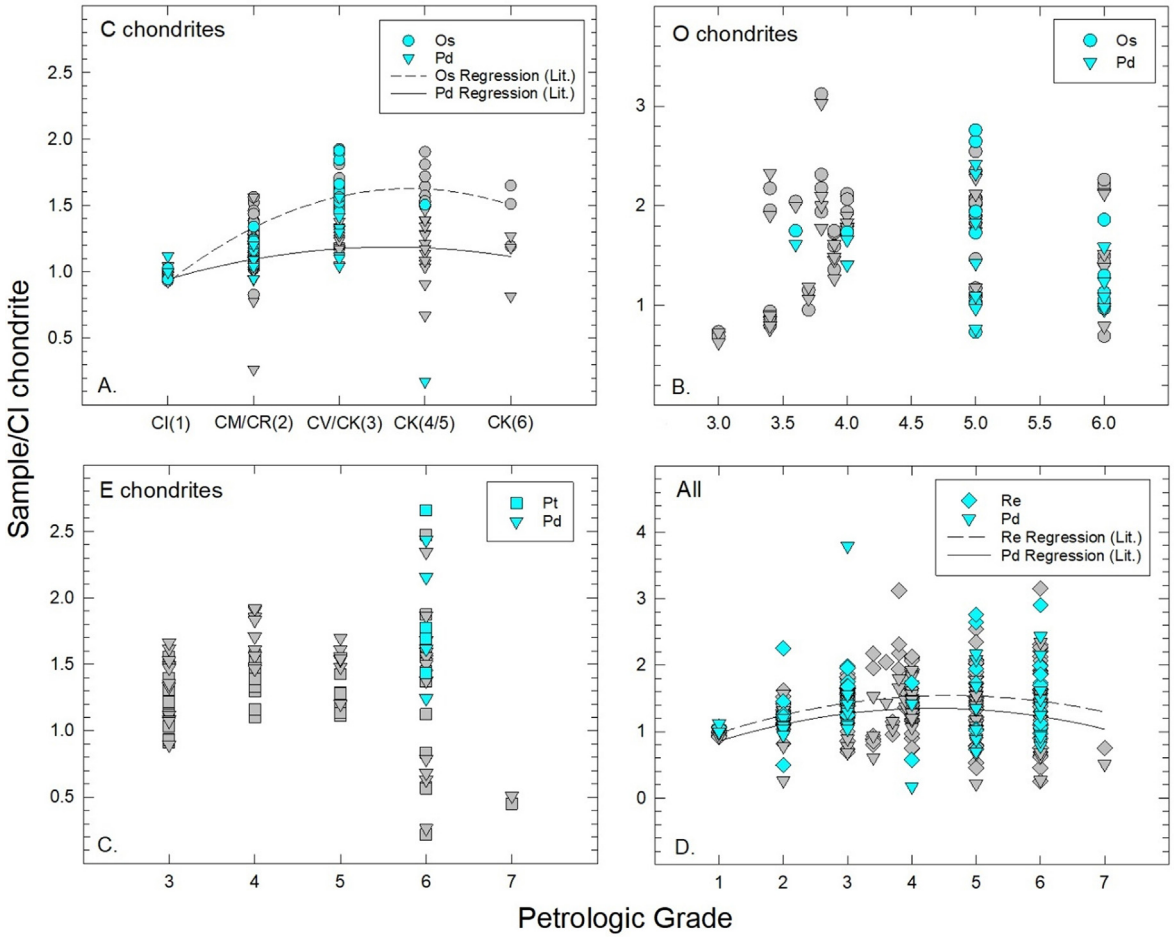

Fig. 13. Plots of normalized HSE abundances versus petrologic type in each class of chondrite, and for all chondrite classes. Teal symbols are representative of data from this study, grey symbols are from previous studies. 2nd order regression lines of the literature (Lit.) data have been plotted for carbonaceous chondrites (A) and for all classes of chondrites (D). Literature data included is sourced from Walker et al., (2002); Horan et al., (2003); Brandon et al., (2005a); Fischer-Gödde et al., (2010); van Acken et al., (2011); Goderis et al., (2017). Figure modified after Day et al., (2016b). Normalization scheme is the same as for Fig. 11.

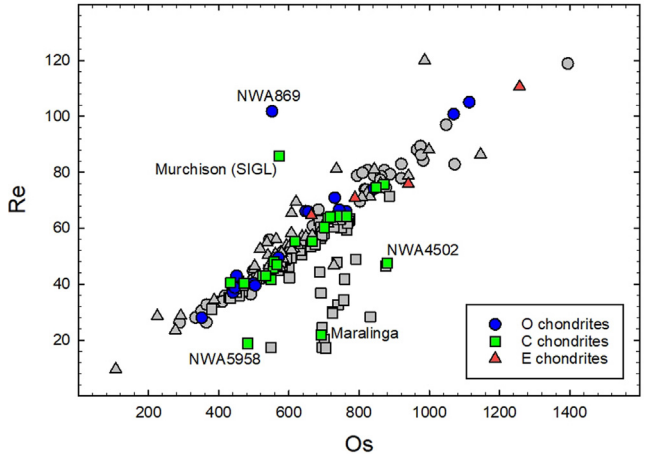

Fig. 14. Plot of rhenium versus osmium (in ppb) for ordinary, carbonaceous and enstatite chondrites (excluding Gujba). Colored symbols are from this study. Samples with suspected terrestrial alteration are labeled with their sample ID. Grey symbols are data from Horan et al., (2003); Fischer-Gödde et al., (2010); Walker et al., (2002); Brandon et al., (2005a); Walker et al., (2018); van Acken et al., (2011); Goderis et al., (2017).

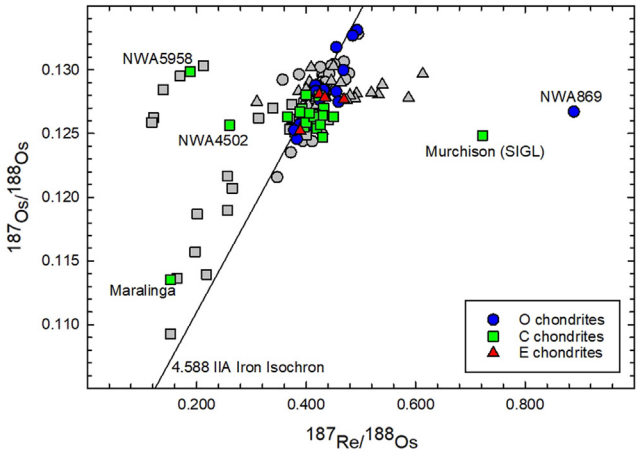

Fig. 15. $^{187}Re/^{188}Os$ versus $^{187}Os/^{188}Os$ for bulk chondrite samples. Colored symbols show data from this study. Grey symbols represent data from Horan et al., (2003); Fischer-Gödde et al., (2010); Walker et al., (2002); Brandon et al. (2005a,b); Walker et al., (2018); van Acken et al., (2011); Goderis et al., (2017). The 4.558 IIIA iron isochron is from Smoliar et al., (1996). Samples of interest from this study are labeled. Note that samples which fall off the 4.558 IIA iron isochron in this figure are also displaced from the grouping of samples in Fig. 14.

for each class vary, where the carbonaceous chondrites show the most significant range. However, when the lowest $^{187}Os/^{188}Os$ ratios are excluded (Maralinga CK4-an (from this study)), the ordinary chondrite class shows the greatest variance between samples (Fig. 18).

5. DISCUSSION

5.1. Nugget heterogeneity and implications for asteroid sampling

For this study, a diversity of chondrite meteorites were examined, mainly to complement those already studied by previous works. For some of these samples only limited initial masses were available for study. For the bulk rock analyses, on average ~0.1 g of sample powder was prepared, with some available sample masses being significantly more limited (<0.02 g) (Table 1). This small sampling method enables evaluation of nugget heterogeneities, such as high HSE contents from metal-rich chondrites, including Gujba. The approach can also enable evaluation of elemental distribution in chondrites. For example, the new HSE results presented here show a similar range of absolute abundance variability – between 28% and 36% - for individual chondrite groups as observed in prior studies that may have examined larger sample powder aliquots. These results suggest a relatively even distribution of the HSE at sub-centimeter to sub-millimeter scales in chondrite meteorites.

While nugget heterogeneity is well known for the HSE in planetary materials (e.g., Day, 2016), it may also occur for other trace and major elements, such as in GRA 06101, as noted above. This effect has the advantage that the results can help to express the degree of trace element fractionation at small scales, but a disadvantage that the compositions of such fragments cannot be taken as the 'bulk composition' of the chondrite. Collectively, the variable sample masses analyzed strongly suggest that variability in elemental abundances in chondrites broadly occurs at masses less than 0.1 g. This information is important for understanding elemental distributions from fine-grained particles accreting to the Earth as well as for sample-return missions such as Osiris-Rex or Hayabusa and Hayabusa-2, for which sample masses of early nebula materials are likely to be finite. In general, when conducting bulk analysis on planetary materials, great care is taken to homogenize powdered samples, yet when sampling chondrite meteorite aliquots < 0.1 g in size, there strong evidence for a 'mode effect', where non-representative fractions of rock samples are measured. This effect may be critical as return sample masses from missions are likely to be finite and curatorial processing may prevent production of homogeneous sample powders. Methods which allow analysis on multiple elemental and isotopic compositions could help aid in discussions revolving around bulk sample or parent body processes which could be misinterpreted if small sample masses produce divergent results.

5.2. Role of terrestrial alteration on chondrite meteorite compositions

Many of the studied meteorites are finds and show evidence of terrestrial alteration. For example, samples found in hot desert environments (e.g., "NWA" samples) can exhibit significant terrestrial alteration effects, drastically modifying the primary abundances of elements which can otherwise provide information on parent body processes (e.g., Crozaz et al., 2003). Past studies have shown evidence of terrestrial alteration in chondrites to be correlated with increases in Ca, Ba, Sr, U, Pb and As abundances, as well as higher abundances of the light REE (LREE) compared to the heavy REE (HREE) (e.g., Crozaz et al., 2003; Lee and Bland, 2004; Al-Kathiri et al., 2005). From the samples examined, the Northwest Africa ordinary (NWA 869) and carbonaceous chondrites (NWA 5958) show relative enrichments in Ba, U and Sr and depletions in Rb relative to CI chondrite (Figs. 6 and 7). These can be explained by small

quantities of terrestrial alteration. Critically, several of the 'non-hot-desert' carbonaceous and ordinary chondrite falls and finds also have Ba and U enrichments, which are more challenging to explain by long-term residence on Earth. Another unusual feature of the new dataset is the general incompatible trace element enrichment observed in the aliquot of Murray (CM). As Murray is a fall, these features are more difficult to explain by terrestrial alteration. Given the sensitivity of Rb and Sr to terrestrial alteration, the Rb-Sr isotope system could be used to further examine trace element disturbance by examining recent disturbance from the Rb-Sr isochron. In these diagrams, NWA 869 and NWA 5958 do not appear strongly disturbed, whereas Äir and Saratov, as well as Murray are displaced from the regression lines in Fig. 9. From this evidence it is likely that the variation in trace elements observed in Murray, as well as Äir and Saratov likely derive from parent body processes, rather than terrestrial alteration.

All three NWA chondrites analyzed in this study (NWA 4502 [CV2], NWA 5958 [C2] and NWA 869 [L3-6]) have Re-Os isotope systematics that deviate significantly from other chondrites which scatter around the expected ~4.56 Ga IIIA Iron isochron (Fig. 15). As would be expected, these chondrites also depart from the chondrite correlation for bulk sample Re and Os compositions (Fig. 14). It has previously been shown that the Re-Os isotope system is susceptible to modification by terrestrial alteration in both chondrite and primitive achondrite meteorites (e.g., Day et al., 2016b; Hyde et al., 2014; Archer et al., 2014; Rankenburg et al., 2007; Fischer-Gödde et al., 2010). Deviations from the $^{187}Re/^{188}Os$ versus $^{187}Os/^{188}Os$ 4.558 IIIA Iron isochron are considered indicators of very recent open-system behavior of Re and/or Os during terrestrial alteration. The greater likelihood is for Re mobilization, rather than that of Os, given the chondritic Os/Ir ratios preserved in these meteorites. For example, the fragment of NWA 869 analyzed experienced apparent Re gain while two carbonaceous chondrites, NWA 4502 and NWA 5958, seem to have experienced Re loss. These behaviors have previously been explained by localized mobilization of Re in sulfides and/or metals in achondrite meteorites (Hyde et al., 2014).

In addition to the NWA chondrites, two other chondrites in this new dataset have strongly disturbed Re-Os isotope systematics. Maralinga is a CK4 find from Australia and has experienced apparent Re-loss, as also observed for NWA 4502 and NWA 5958. Murchison, on the other hand, is a CM2 fall and from Australia, but one of the two fragments that we measured had anomalously high Re (Re – 85.8 μg/g; $^{187}Re/^{188}Os$ – 0.722). A recent study of the Sutter's Mill carbonaceous chondrite has shown that redistribution of Re, and possibly minor quantities of Os, occurred prior to collection of meteorite fragments, during a timeframe of a few hours to days of rainy weather (Walker et al., 2018). As with achondrites (Hyde et al., 2014), Walker et al., (2018) found that Re is the most vulnerable of the HSE to terrestrial effects. The results from Sutter's Mill suggest that a fall, including Maralinga, or even finds, such as Murchison, do not require much time, either before collection or perhaps even during curation, to experience even minor perturbations to elements associated with sulfide or metal phases, or to elements that may also be hydrophile (e.g., halogens, large ion lithophile elements). Although the cause of the Re enrichment in the Murchison (Lab ID = SIGL) sample remains a mystery, like previous studies, the enrichments seen in this Murchison sample are not always reproducible for other Murchison powders analyzed and therefore it is unclear as to if the results are from heterogeneous distribution on the parent body, or are due to terrestrial weathering (Braukmüller et al., 2018).

5.3. High field strength elements in chondrites and the Ivuna composition

New data for mineral phases in the Chelyabinsk chondrite, normalized to CI chondrite Ivuna (Barrat et al., 2012), show relative and absolute abundances of the REE and incompatible trace elements similar to mineral phases normally found in ordinary chondrites. However, anomalous behavior is exhibited for the high field strength elements (HFSE), showing positive anomalies in Zr, Hf, Nb and Ta for the chondrule, pyroxene, olivine and the fusion crust separates, and negative anomalies for Zr, Hf and Nb for the phosphate analyses, when normalized to carbonaceous Ivuna abundances from Barrat et al., (2012). Minor anomalies in the HFSE, relative to the same normalization are also evident in some bulk chondrite measurements (e.g., Allende, Chelyabinsk, Forest City and the enstatite chondrites that were measured). Recently, three studies, including this study, have reported new trace element abundance measurements in Ivuna (this study, Barrat et al., 2012; Braukmüller et al., 2018), expanding on the preferred CI value reported by McDonough and Sun (1995) (Table 8). Comparison of the new Ivuna data with these prior studies shows that the fragments analyzed here have higher P, Ba and Ta, and higher absolute abundances than in Barrat et al., (2012) and Braukmüller et al., (2018) (Fig. 16). In particular, the HFSE in analyses by the prior studies are between ~10 and 30% lower than here, or in the compilation of McDonough and Sun (1995), yet adjacent elements on the comparison plots (U, La, Nd and Sm) are similar.

Both this study and Braukmüller et al., (2018) performed Paar bomb digestion for Ivuna, which is a highly effective method for complete digestion. Conventional dissolutions in Teflon vials, on the other hand, can be less reliable at digesting refractory mineral phases, such as zircon. These differences in digestion method may be a source of minor discrepancy between the results of this study, Braukmüller et al., (2018) and Barrat et al., (2012), where the latter did not use Paar bomb digestion. Alternatively, there may also be localized heterogeneity in Ivuna fragments. In all cases, using Ivuna values from these studies still leads to minor HFSE anomalies observed in the Chelyabinsk components and in some chondrites. These observations support some variability in HFSE within chondrites and chondrite groups. Absent of obvious terrestrial modification effects, one possibility to explain these small variations are parent body alteration processes wherein HFSE are immobile relative to elements of similar incompatibility

Table 8
Compositional data for Carbonaceous Ivuna chondrite.

Sample		Ivuna		CI	Ivuna	Ivuna
Method		Paar Bomb		Compilation	Hotplate	Paar Bomb
Study		This study	*2SD*	[1]	[2]	[3]
Fe	wt.%	26.7	*0.5*	18.1		18.2
P	wt.%	0.259	*0.004*	0.108	0.106	0.085
Ti	wt.%	0.035	*0.001*	0.044		0.038
Mn	wt.%	0.251	*0.006*	0.192	0.200	0.204
Cr	wt.%	0.231	*0.002*	0.265		0.258
Co	wt.%	0.060	*0.003*	0.050	0.055	0.051
Ni	wt.%	1.21	*0.06*	1.05		1.12
Li	μg/g	1.36	*0.01*	1.5	1.44	
Sc	μg/g	6.08	*0.15*	5.92	6.08	
V	μg/g	44.6	*1.5*	56	54.0	47.5
Cu	μg/g	114.5	*2.6*	120	138	136
Zn	μg/g	407.0	*5.1*	310	330	321
Ga	μg/g	10.9	*0.5*	9.2	9.7	8.7
Ge	μg/g	23.8	*1.7*	31		
Se	μg/g	1.45	*0.03*	21		
Rb	μg/g	2.37	*0.01*	2.30	2.23	2.09
Sr	μg/g	5.6	*0.1*	7.3	8.0	
Y	μg/g	1.65	*0.15*	1.57	1.60	
Zr	μg/g	3.61	*0.25*	3.82	3.48	3.27
Nb	μg/g	0.30	*0.01*	0.24	0.30	0.25
Mo	μg/g	1.31	*0.08*	0.90		
Sn	μg/g	1.65	*0.04*	1.65		1.48
Cs	μg/g	0.248	*0.008*	0.190	0.192	0.173
Ba	μg/g	4.24	*0.03*	2.41	2.57	2.20
La	μg/g	0.226	*0.001*	0.237	0.241	0.189
Ce	μg/g	0.56	*0.04*	0.61	0.61	0.50
Pr	μg/g	0.086	*0.005*	0.093	0.092	0.082
Nd	μg/g	0.456	*0.038*	0.457	0.471	0.428
Sm	μg/g	0.152	*0.013*	0.148	0.155	0.144
Eu	μg/g	0.051	*0.002*	0.056	0.060	0.055
Gd	μg/g	0.225	*0.016*	0.199	0.213	0.212
Tb	μg/g	0.0406	*0.0011*	0.0361	0.0388	0.0356
Dy	μg/g	0.276	*0.014*	0.246	0.260	0.243
Ho	μg/g	0.0613	*0.0001*	0.0546	0.0579	
Er	μg/g	0.1857	*0.0014*	0.1600	0.1700	0.1580
Tm	μg/g	0.0287	*0.0015*	0.0247	0.0271	0.0243
Yb	μg/g	0.183	*0.008*	0.161	0.171	0.165
Lu	μg/g	0.0293	*0.0024*	0.0246	0.0248	0.0242
Hf	μg/g	0.11692	*0.00002*	0.103	0.107	0.096
Ta	μg/g	0.0232	*0.0015*	0.0136	0.0149	
W	μg/g	0.105	*0.009*	0.093	0.10	0.09
Pb	μg/g	2.68	*0.02*	2.47	2.65	2.39
Th	μg/g	0.0325	*0.0005*	0.0290	0.0289	0.0251
U	μg/g	0.0083	*0.0003*	0.0074	0.0075	0.0060

Data are from this study and [1] McDonough and Sun, 1995 [2] Barrat et al., 2012 [3] Braukmüller et al., 2018.

(e.g., REE), leading to minor variability in these elements. The variability in HFSE is particularly evident in enstatite chondrites, or in chondrites measured with limited powdered sample masses, reflecting that any HFSE versus REE mobility in chondrites occurring during thermal metamorphism spanned limited length-scales (Fig. 17).

5.4. Role of parent body processes on chemical component distribution in chondrites

Major processes thought to act on chondrite parent bodies after their accretion include thermal metamorphic processes, as well as aqueous and fluid alteration (e.g., Brearley and Jones, 1998). Many of these processes are likely to have been operative within the first few million years of the evolution of chondrite parent bodies, whereas metamorphism can continue to occur later due to disruptive collisions between bodies. In this study, samples analyzed span a wide range of apparent alteration states and thermal metamorphic grades (Table S1). Despite this, we find that the trace element abundances for the majority of the carbonaceous chondrites are considered to be similar to those measured in CI-chondrite Ivuna. This data would support the suggestion that secondary processes, such as thermal metamorphism on the parent body, have only had minor effects on the relative abundances of elements and the bulk

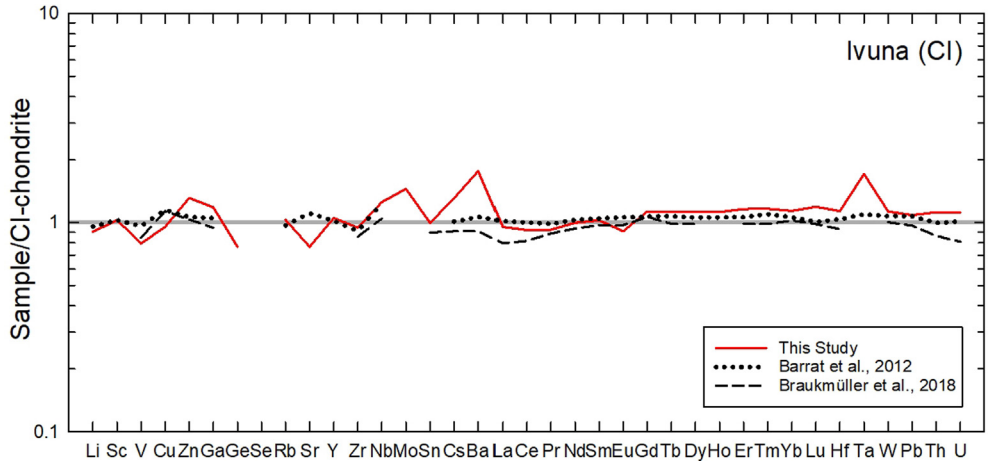

Fig. 16. Comparisons of Ivuna trace element chemistry. Data from this study, Braukmüller et al., (2018) and Barrat et al., (2012) have been normalized to the CI compilation from McDonough and Sun (1995).

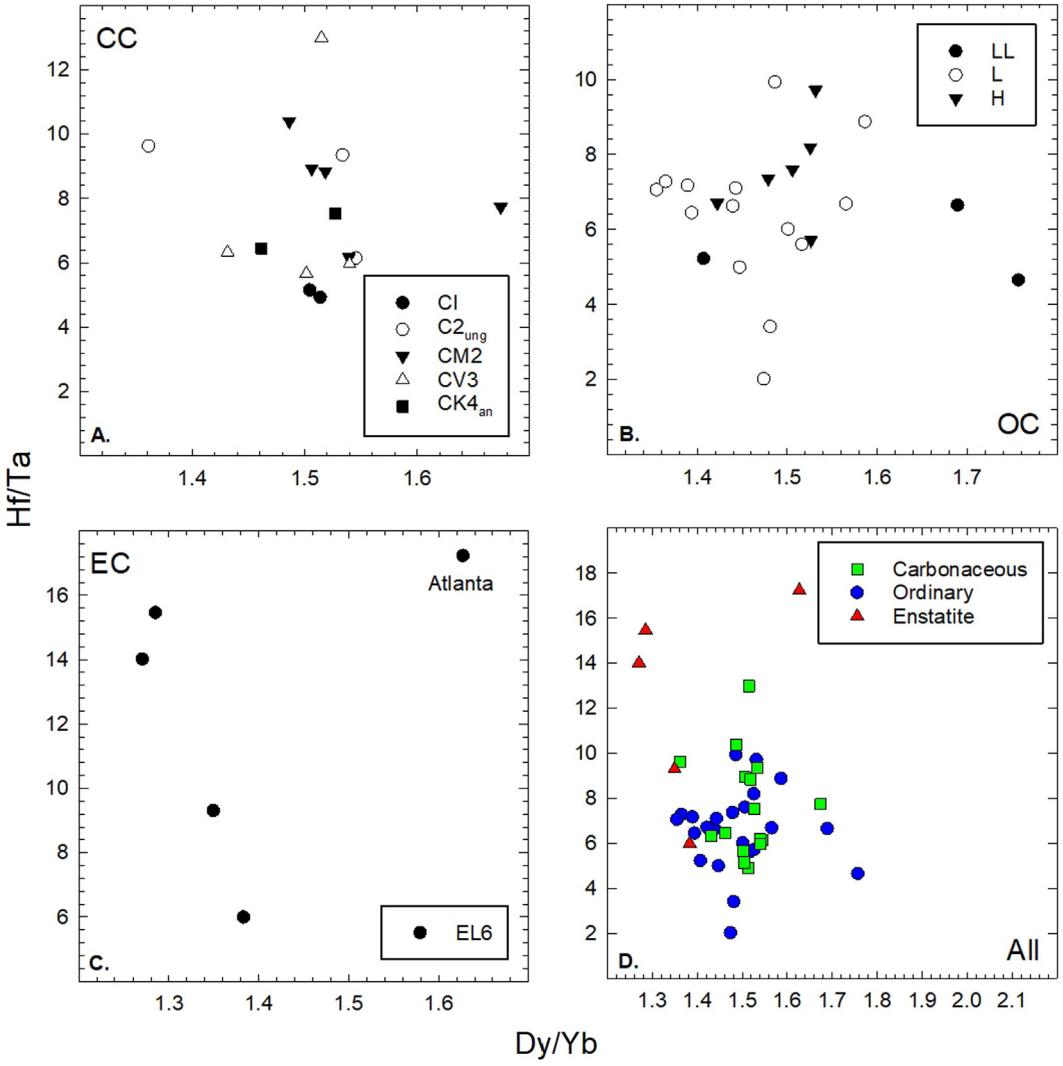

Fig. 17. Dy/Yb versus Hf/Ta ratios for the chondrite classes. Data are from this study.

composition of carbonaceous chondrites (Braukmüller et al., 2018) and supports the limited spatial distribution at which such processes are likely to be operative.

In contrast to carbonaceous chondrites, EL6 chondrites are considered be strongly affected by brecciation and/or impact melting (e.g., Rubin et al., 2009; Barrat et al., 2014). Trace element abundance data from previous studies have shown negative Sm and Yb anomalies, thought to be a nebular signature in EH3 and EL3 residues. However, no such anomalies are seen in the EL6 sample, indicating that such signatures may have been erased through metamorphism or impact melting processes (Barrat et al., 2014). While previous studies have suggested that all EL chondrites belong to the same metamorphic grade, the lack of diversity among this sample suite for enstatite chondrites does not enable consideration of their relationships. Rubin et al., (2009), suggested that EL6 chondrites could be compositional residues of EL3 chondrites after the extraction of plagioclase- and oldhamite-bearing melt. Calcium-depletion in EL6 chondrites is necessary for this model, but even so, it is difficult to support (Barrat et al., 2014).

Thermal metamorphism does not seem to have a significant effect on the HSE distribution within chondritic parent bodies. Carbonaceous chondrites show an increasing abundance of Os and Pd with an increase in petrologic type; however, as these samples have experienced limited parent body processing, this would seem to reflect a dilutional effect from volatile retention and release rather than HSE mobility (Day, 2016; Fig. 13A.). Enstatite chondrites from this study show that there is more variation in Pt and Pd abundances in the EL group than previously measured (Fig. 13C.). Overall, Re and Pd within all chondrite classes remains constant through parent body processing, suggesting that mobilization of these elements is affected through a subsequent process.

As with past studies, we find major element compositional relationships between different chondrite groups (Fig. 5). C2 and CM2 chondrites from this study fall to the left of the main trend seen in the same samples from past studies (Alexander, 2019a,b). The compositional variations of these carbonaceous chondrite groups are suggestive of Mg-loss from hydration. Past studies have suggested that carbonaceous chondrites hold most of the water in the structural bonds of phyllosilicates that formed during aqueous alteration of anhydrous minerals, such as olivine and pyroxene, on their parent bodies (Greshake, 2014; Brearley, 2006). Given that the samples from this study were of petrologic grade "2″ their assumed "lesser" geochemical processing would corroborate with the presence of fewer hydrous materials.

Considering that the above discussion is based on bulk sample analysis, care was taken to consider the various mineral phases of the Chelyabinsk chondrite to reveal further information on potential formational environments of its metals and its parent body processes. The HSE abundances of the various components of the Chelyabinsk chondrite give information on the mobility of these elements during accretionary and parent body processing. Two types of metals were measured in the Chelyabinsk chondrite. The type-1 metal contained higher concentrations of Pd and Au, previous studies show that high-Ni metals in chondrites contain higher Pd and Au relative to low-Ni metals while the remaining HSE remain nearly unfractionated between the two groups (Campbell and Humayun, 2003) Furthermore, previous studies have shown that this pattern of the HSE is like those observed for kamacite-taenite partitioning from subsolidus reactions in ordinary chondrites and iron meteorites (e.g., Narayan and Goldstein, 1985; Campbell and Humayun, 1999). The refractory HSE are nearly the same for both metals suggesting equilibration, likely between the kamacite and taenite. Slow cooling allows these metal phases to equilibrate, and since Ni partitions more readily into liquid metal, the Ni contents of both phases would have increased (Campbell and Humayun, 2003).

5.5. The HSE content and Pt/Os, Re/Os, Pd/Ir and Ru/Ir of chondrites

Carbonaceous chondrites from this study show, on average, ~8% lower Re/Os than those of ordinary or enstatite chondrites, agreeing well with previous studies (Walker et al., 2002; Horan et al., 2003). The lower average $^{187}Os/^{188}Os$ ratios of this class of meteorites indicates that this difference is a long-term effect (e.g., Walker et al., 2002; Horan et al., 2003) caused during the formation of the meteorite group. An argument has been made that the fractionation is due to early, high-temperature fractionation in the solar nebula (e.g., Horan et al., 2003) and is corroborated by studies such as Sylvester et al., (1990) and (1993), where Fremdlinge from CV3 chondrites showed sub-chondritic Re/Os ratios. These Fremdlinge measurements have been used in thermodynamic modeling, resulting in data consistent with solar nebula processing (Berg et al., 2009), where refractory metal alloys were recovered and measured for Os, W, Mo and Ru to display evidence for nebular condensation formation processes (Fischer-Gödde et al., 2010). These features are consistent with processing within inner and outer Solar System reservoirs held to be responsible for the compositional differences observed in carbonaceous versus ordinary and enstatite meteorite groups (e.g., Warren, 2011; Kruijer et al., 2017).

Maralinga (CK4an) is a unique sample from the suite of carbonaceous chondrites regarding its Re abundance and Re-Os isotopic compositions. Its low Re content (21.8 ng g^{-1}) and $^{187}Re/^{188}Os$ (0.152) ratio yield one of the lowest $^{187}Os/^{188}Os$ (0.11351) ratios ever measured for a chondrite meteorite. Maralinga has been described previously as a petrologically anomalous sample. Petrologic observations have shown that Maralinga contains ~50% matrix, ~50% chondrules and 3% CAIs (Keller et al., 1992); this is starkly different to the mean CK chondritic values of ~75% matrix, ~15% chondrules and rare CAIs (0.5%) (Krot et al., 2004). Notably, previous studies have reported Maralinga to have a high Ni content in its olivine, pentlandite, ilmenite, magnetite and pyroxenes when comparing to other CK chondrites (e.g., Noguchi, 1993; Dunn et al., 2016). However, when considering all carbonaceous chondrites from our bulk sample major element analysis, Maralinga has one of the lowest Ni contents. This could be a result of processes

invoked by various studies showing CK chondrites to contain only minor amounts of FeNi metal (Fischer-Gödde et al., 2010). It has been shown that most of the metal in these samples has been oxidized, resulting in the formation of secondary phases like magnetite, FeO-rich silicates and HSE-rich sulfides, tellurides and arsenides (e.g., Geiger and Bischoff, 1989; Kallemeyn et al., 1991; Choi and Wasson, 2003). Overall, the relative enrichment of trace elements in Maralinga could be suggestive of a low degree of parent body thermal metamorphism. This scenario may be further supported from previous studies measurements of Maralinga's high Ni content in many of its minerals, suggesting un-equilibrated fine-grained phases in the matrix compared to those measured in other CK-chondrites (e.g., Geiger and Bischoff, 1989; Huber et al., 2006).

Generally, measurements of HSE in ordinary chondrites show decreasing HSE abundance from H > L > LL, which is consistent with increasing HSE partitioning into metal phases and the respective metal content in these meteorite classes. The Re and Os concentrations of ordinary chondrites are generally higher than those of the other groups measured in this study, likely due to their higher metal content than other groups. New HSE data from this study agrees with previous conclusions that petrologic type (Fig. 13B) does correlate to refractory elements in bulk rocks and therefore it is unlikely that isochemical thermal metamorphism had a significant effect on these samples (e.g., Fischer-Gödde et al., 2010; Kallemeyn et al., 1989; van Acken et al., 2011). As suggested by Fischer-Gödde et al., 2010, the process that led to high or low metal abundances within ordinary chondrites did not pointedly fractionate the HSE from each other. It becomes possible then, that the HSE patterns seen in ordinary chondrites were established before the parent bodies of the ordinary chondrites were formed.

The HSE abundance data from the four enstatite chondrite meteorite samples measured in this study agree relatively well with previous studies. Khairpur (EL6) shows anomalously high abundances compared to the other samples and previous measurements on various enstatite chondrites (Fig. 12C.). The HSE abundances in EL chondrites measured from this study show similar compositions to both EL and EH chondrites from previous studies (e.g., Horan et al., 2003; Fischer-Gödde et al., 2010). These data would suggest that the HSE fractionation processes that occurred in EL chondrites were likely occurring in EH chondrites as well.

5.6. Implications for planetary feedstocks

The history of planets, such as Earth, can be discussed through the information provided by chondrites. Considering that HSE partition into metal phases during metal-silicate equilibration, it is expected that these elements would be sequestered to the Earth's core. However, measured HSE abundances in the bulk silicate Earth are higher than predicted by metal-silicate partitioning experiments (e.g., Day et al., 2016b; Mann et al., 2012). These elevated abundances of the HSE in the bulk silicate Earth are thought to have occurred through late accretion of primitive material after core formation (e.g., Kimura et al., 1974; Chou, 1974; Day et al., 2016b; Hopp and Kleine, 2018; Fischer-Gödde and Kleine, 2017; Fischer-Gödde et al., 2020). It has been argued that during late accretion, approximately ~0.5 wt.% of chondritic material was added to the bulk silicate Earth (Day et al., 2016b *and references therein*). Additionally, a report by Özdemir et al., 2019 documented that HSE were added to Earth in Archean times in the form of chondrites. However, the nature of this late-accreted chondritic material, whether it was carbonaceous, ordinary, enstatite, or compositionally distinct from measured chondrites, remains debated.

Studies including Walker et al., (2002) and Meisel et al., (1996) suggest, based on Os isotopes and HSE abundances that enstatite or ordinary chondrite compositions are likely to be representative of the late accretionary material to the Earth. Platinum-osmium and rhenium-osmium isotope data support similar compositions (e.g., Brandon et al., 2005a, 2005b, Day et al., 2017a, 2017b). Conversely, other studies, that are also based on Os isotopes and HSE abundances, suggest that the source of this late accretionary material is a carbonaceous chondrite-like material with chemically evolved metal components, such as those seen in some iron meteorites (Fischer-Gödde et al., 2012). To further compound this issue, data on lunar impact melt breccias imply an entirely different population of impactors from modern chondrites striking the Moon at 3.8 Ga (e.g., Puchtel et al., 2008; McIntosh et al., 2020). Having a better understanding of the type of late accretionary material that was likely added to Earth is important to understanding, not only the late-stage of planetary formation, but could also to link the source of Earth's water and highly volatile element compositions (Wang and Becker, 2013).

Ordinary chondrites represent approximately 80% of the observed modern chondritic falls (Kallemeyn et al., 1989) and are thought to originate from the inner portion of the asteroid belt (Rubin, 2013). Recent discovery of dozens of ordinary chondrites within 470 Ma sedimentary rocks in Sweden, suggesting that ordinary chondrites have been falling to Earth for more than 10% of the planet's history (Schmitz et al., 2016). It would therefore seem, that the ordinary chondrite class could be one of the more significant sources for HSE abundances in the bulk silicate Earth. The new $^{187}Os/^{188}Os$ data from this study supports similarities between ordinary chondrites and bulk silicate Earth (Fig. 18).

Carbonaceous chondrites, on the other hand make up approximately 5% of chondritic falls (Kallemeyn and Wasson, 1981). The high abundance of organic compounds often found in this class would suggest an origin further from the Sun than that of the ordinary chondrites (Rubin, 2013). Given the hypothesized regions of the Solar System that these chondrites are sourced from, it is less likely that the carbonaceous chondrite groups contributed significantly to late-accretion addition of the HSE. Marty (2012) demonstrated through stable and noble gas isotopes that the source of Earth's volatiles is likely chondritic. Furthermore, the study noted that the fraction of water and carbon incorporated in the Earth versus the higher noble gas concentrations in the atmosphere, is representative of active exchanges of volatile elements between the mantle

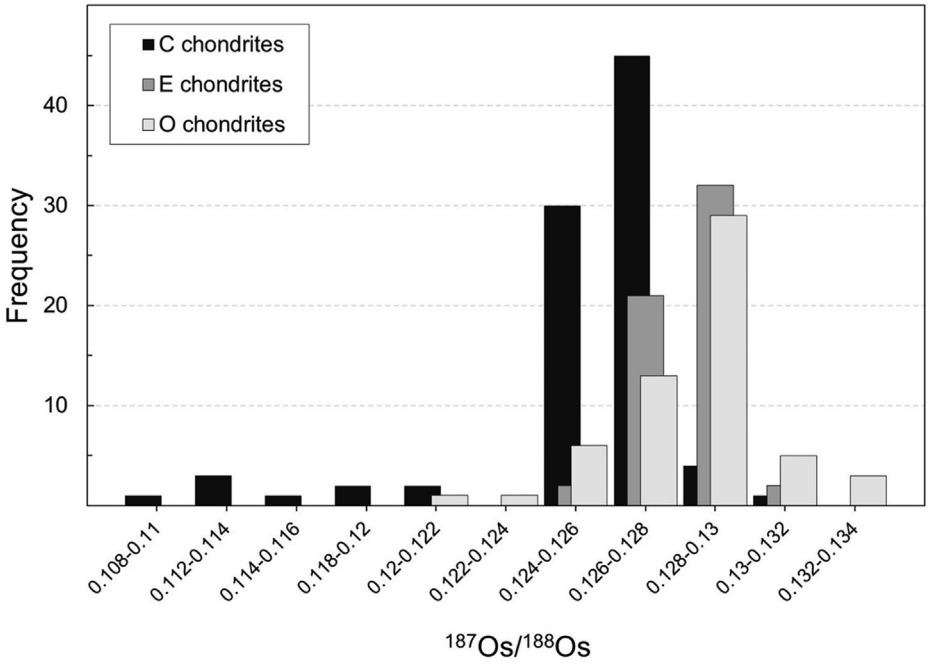

Fig. 18. Histogram of $^{187}Os/^{188}Os$ ratios for chondrite classes. Data are from this study, Horan et al., (2003); Fischer-Gödde et al., (2010); Walker et al., (2002); Brandon et al. (2005a,b); Walker et al., (2018); van Acken et al., (2011) and Goderis et al., (2017).

and the surface of the Earth. This high water and carbon concentration of bulk silicate Earth would suggest that the accretion of volatile elements from wet planetesimals occurred during the main Earth forming event, rather than a contribution of wet late-accretionary material, such as carbonaceous chondrites (Marty, 2012).

Enstatite chondrites make up approximately 2% of the chondritic falls (Rubin, 2013). These rare chondrites are thought to be sourced from the orbit of Mars, considerably closer to the Sun than other chondritic groups (e.g., Kallemeyn and Wasson, 1986; Rubin, 2013). Multiple studies have shown that enstatite chondrites are elementally and isotopically similar to Earth's bulk composition (Javoy et al., 2010; Dauphas, 2017; Fischer-Gödde and Kleine, 2017; Fischer-Gödde et al., 2020). Dauphas (2017) developed models which determined that the isotopic signatures of lithophile (O, Ca, Ti and Nd), moderately siderophile (Cr, Ni and Mo) and highly siderophile (Ru) elements for bulk Earth were most similar to those of enstatite chondrites. Ruthenium isotope measurements reported by Fischer-Gödde and Kleine (2017) further support these models showing that the magnitude of $\varepsilon^{100}Ru$ anomalies in enstatite chondrites were closest to terrestrial values compared with other chondrite groups. Considering these studies, the contribution of enstatite chondrite feedstocks to the early Earth may have been significant and that the current in fall of chondrite types are not necessarily representative of the earlier planetary feedstocks.

The relationships in Fig. 19 provide insight, as the high $^{87}Sr/^{86}Sr$ ratios in ordinary and enstatite groups indicate

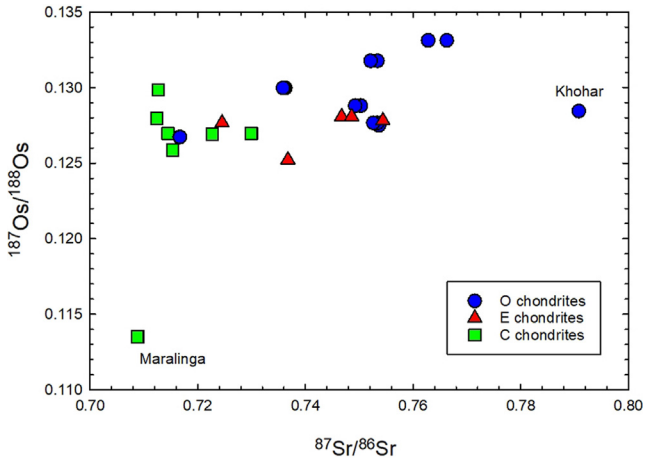

Fig. 19. Measured $^{87}Sr/^{86}Sr$ versus $^{187}Os/^{188}Os$ for chondrites from this study.

that they have high Rb/Sr compositions. If these groups are responsible for contributing materials to Earth after the main phases of core formation, they could also be responsible for adding, to an extent, the volatile elements as well. Considering this, if no volatile loss occurred during the late accretionary delivery and a 0.5% mass addition is assumed, the Rb/Sr ratio of the Earth should have changed by approximately 2.2% by addition of ordinary chondrites, or 2% for enstatite chondrites, versus only 1.6% by addition of carbonaceous chondrites. This would make the pre-late accretion $^{87}Sr/^{86}Sr$ composition of the bulk silicate Earth marginally lower than the estimated bulk silicate Earth based on the modern mantle $^{87}Sr/^{86}Sr$ estimate of 0.7047 (e.g., Caro and Bourdon, 2010). These observations are consistent with recent work that suggest ordinary chondrites could have delivered a significant volatile fraction to the Earth during late accretion (e.g., Peslier, 2020).

6. CONCLUSIONS

This study reports a combined data set of major-, trace- and highly siderophile elements, along with Rb-Sr and Re-Os isotope systematics for 12 ordinary-, 13 carbonaceous- and four enstatite-chondrites. Along with new O-isotope data, these results: (i) extend the known range of HSE and Re-Os isotope data for chondrites; (ii) provide a coherent suite of combined elemental and isotopic data to examine chondrites and (iii) reports new mineral-chemical data for the Chelyabinsk LL5 ordinary chondrite fall for comparison with these data. The major conclusions of this study are:

(1) Nugget heterogeneity for the HSE, which are particularly susceptible to uneven distribution in chondrite components is most significant in powder aliquots less than 0.1 g. This value provides a useful threshold for examining chondritic materials from missions such as Osiris-Rex and Hayabusa-2.
(2) Terrestrial alteration effects in chondrites are pronounced in hot desert samples for certain elements (Ba, U, Sr), but also occur in carbonaceous chondrite falls, where Re/Os disturbance can occur either in the short time between fall and collection, or perhaps even during curation, supporting recent observations of similar disturbance in the Sutter's Mill chondrite fall (Walker et al., 2018).
(3) High field strength element (Ti, Zr, Ta, Nb, Hf) abundances can be quite variable in chondrites, especially in comparison of carbonaceous chondrite Ivuna compositions (this study; Barrat et al., 2012; Braukmüller et al., 2018). Due to the potential for these elements to be within refractory mineral reservoirs in chondrites (e.g., Zr-rich phases), complete digestion is important for examining their variations in chondrites.
(4) Parent-body processes are responsible for many of the subtle geochemical variations observed in chondrites, and dehydration may have an important role of the relative and absolute abundances of the HSE. Parent-body processes, however, cannot explain the distinct Rb-Sr and Re-Os isotope systematics of chondrite groups.
(5) The distinct long-term Re/Os ratio of ordinary chondrites, ~8% higher than for carbonaceous chondrites, make them a more likely source for the higher $^{187}Os/^{188}Os$ of the bulk silicate Earth. Their long-term elevated Rb/Sr ratios also make them a potentially moderately volatile-rich feed-stock during late accretion.

Declaration of Competing Interest

The authors declare that they have no known competing financial interests or personal relationships that could have appeared to influence the work reported in this paper.

ACKNOWLEDGMENTS

This work was made possible through support from the NASA Emerging Worlds program (80NSSC19K0932). We acknowledge Larry Taylor for prompting study of the Chelyabinsk meteorite. The review comments of T. Dunn and M. Fischer-Gödde are gratefully acknowledged.

APPENDIX A. SUPPLEMENTARY MATERIAL

Supplementary data to this article can be found online at https://doi.org/10.1016/j.gca.2021.11.020.

REFERENCES

Afiattalab F. and Wasson J. T. (1980) Composition of the metal phases in ordinary chondrites: Implications regarding classification and metamorphism. *Geochim. Cosmochim. Acta* **44**, 431–446.

Alexander C. M. O'D. (2019a) Quantitative models for the elemental and isotopic fractionation in chondrites: The carbonaceous chondrites. *Geochim. Cosmochim. Acta* **254**, 277–309.

Alexander C. M. O'D. (2019b) Quantitative models for the elemental and isotopic fractionation in chondrites: The non-carbonaceous chondrites. *Geochim. Cosmochim. Acta* **254**, 246–276.

Al-Kathiri A., Hofmann B. A., Jull A. J. T. and Gnos E. (2005) Weathering of meteorites from Oman: Correlation of chemical and mineralogical weathering proxies 14C terrestrial ages and the influence of soil chemistry. *Met. Planet. Sci.* **40**, 1215–1239.

Anders E. (1971) Meteorites and the early solar system. *Annu. Rev. Astron. Astrophys.* **9**, 1–34.

Anders E. and Grevesse N. (1989) Abundances of the elements: Meteoritic and solar. *Geochim. Cosmochim. Acta* **53**, 197–214.

Archer G. J., Ash R. D., Bullock E. S. and Walker R. J. (2014) Highly siderophile elements and ^{187}Re-^{187}Os isotopic systematics of the Allende meteorite: evidence for primary nebular processes and late-stage alteration. *Geochim. Cosmochim. Acta* **131**, 402–414.

Barrat J. A., Zanda B., Jambon A. and Bollinger C. (2014) The lithophile trace elements in enstatite chondrites. *Geochim. Cosmochim. Acta* **128**, 71–94.

Barrat J. A., Zanda B., Moynier F., Bollinger C., Liorzou C. and Bayon G. (2012) Geochemistry of CI chondrites: Major and trace elements, and Cu and Zn Isotopes. *Geochim. Cosmochim. Acta* **83**, 79–92.

Becker H., Horan M. F., Walker R. J., Gao S., Lorand J.-P. and Rudnick R. L. (2006) Highly siderophile element composition of the Earth's primitive upper mantle: Constraints from new data on peridotite massifs and xenoliths. *Geochim. Cosmochim. Acta* **70**, 4528–4550.

Berg, T., Marosits, E., Maul, J., Schönhense, G., Hoppe, P., Ott, U. and Palme, H. (2009) Evidence for Nebular Condensation of Sub-Micron Refractory Metal Alloys. *Lunar Planet. Sci. XL*. Lunar Planet. Inst., Houston. #1585(abstr.).

Brandon A. D., Humayun M., Puchtel I. S. and Zolensky M. E. (2005a) Re-Os isotopic systematics and platinum group element composition of the Tagish Lake carbonaceous chondrite. *Geochim. Cosmochim. Acta* **69**, 1619–1631.

Brandon A. D., Humayun M., Puchtel I. S., Leya I. and Zolensky M. (2005b) Osmium isotope evidence for an s-process carrier in primitive chondrites. *Science* **309**, 1233–1236.

Braukmüller N., Wombacher F., Hezel D. C., Escoube R. and Münker C. (2018) The chemical composition of carbonaceous chondrites: implication for volatile element depletion, complementarity and alteration. *Geochim. Cosmochim. Acta* **239**, 17–48.

Brearley A.J., Jones R.H. and Papike J.J. (1998) Chondritic meteorites. In *Planetary Materials*, v. 36 Reviews in Minerology.

Brearley A. J. (2006) The action of water. *Meteorites Early Solar Syst. II* **943**, 587–624.

Brown P. G., Assink J. D., Astiz L., Blaauw R., Boslough M. B., Borovicka J., Brachet N., Brown D., Campbell-Brown M., Ceranna L., Cooke W., Groot-Hedlin de C., Drob D. P., Edwards W., Evers L. G., Garces M., Gill J., Hedlin M., Kingery A., Laske G., Le Pichon A., Mialle P., Moser D. E., Saffer A., Silber E., Smets P., Spalding R. E., Spurney P., Tagliaferri E., Uren D., Weryk J., Whitaker R. and Krzeminski Z. (2013) A 500-kiloton airburst over Chelyabinsk and an enhanced hazard from small impactors. *Nature* **503**, 238–241.

Campbell A.J., and Humayun M. (1999) Microanalysis of platinum group elements in iron meteorites using laser anliation ICP-MS. *Lunar and Planet. Sci. XXX*, Lunar Planet. Inst., Houston. #1974(absr.).

Campbell A. J. and Humayun M. (2003) Formation of metal in Grosvenor Mountains 95551 and comparison to ordinary chondrites. *Geochim. Cosmochim. Acta* **67**, 2481–2495.

Caro G. and Bourdon B. (2010) Non-chondritic Sm/Nd ratio in the terrestrial planets: Consequences for the geochemical evolution of the mantle–crust system. *Geochim. Cosmochim. Acta.* **74**, 3333–3349.

Choi B.-G. and Wasson J. T. (2003) Microscale oxygen isotopic exchange and magnetite formation in the Ningqiang anomalous carbonaceous chondrite. *Geochim. Cosmochim. Acta* **67**, 4655–4660.

Chou C.-L. (1974) Fractionation of Siderophile Element Ratios in the Earth's Upper Mantle and Lunar Samples. *Lunar and Planet. Sci. IX*, Lunar Planet. Inst., Houston. #1058(absr.).

Clayton R. N., Mayeda T. K. and Rubin A. E. (1984) Oxygen isotopic compositions of enstatite chondrites and aubrites. *Proc. Lunar and Planet. Sci. XV, in J. Geophys.* **89**, C245–C249.

Clayton R. N. and Mayeda T. K. (1999) Oxygen isotope studies of carbonaceous chondrites. *Geochim. Cosmochim. Acta* **63**, 2089–2014.

Cohen A. S. and Waters F. G. (1996) Separation of osmium from geological materials by solvent extraction for analysis by thermal ionization mass spectrometry. *Anal. Chim. Acta* **332**, 269–275.

Criss R. E. and Farquhar J. (2008) Abundance, notation and fractionation of light stable isotopes. *Rev. Mineral. Geochem.* **68**, 15–30.

Crozaz G., Floss C. and Wadhwa M. (2003) Chemical alteration and REE mobilization in meteorites from hot and cold deserts. *Geochim. Cosmochim. Acta* **67**, 4727–4741.

Daly L., Bland P. A., Dyl K. A., Forman L. V., Evans K. A., Trimby P. W., Moody S., Yang L., Liu H, Ringer S. P., Ryan C. G. and Saunders M. (2017) In situ analysis of refractory metal nuggets in carbonaceous chondrites. *Geochim. Cosmochim. Acta* **216**, 61–81.

Dauphas N. (2017) The isotopic nature of the Earth's accreting material through time. *Nature* **541**, 521–524.

Day J. M. D. (2015) Planet formation processes revealed by meteorites. *Geol. Today* **31**, 12–20.

Day J. M. D., Corder C. A., Rumble, III, D., Assayag N., Cartigny P. and Taylor L. A. (2015) Differentiation processes in FeO-rich asteroids revealed by the achondrite Lewis Cliff 88763. *Meteorit. Planet. Sci.* **50**, 1750–1766.

Day J. M. D., Waters C. L., Schaefer B. F., Walker R. J. and Turner S. (2016a) Use of hydrofluoric acid desilicification in the determination of highly siderophile element abundances and Re-Pt-Os isotope systematics in mafic-ultramafic rocks. *Geostand. Geoanal. Res.* **40**, 49–65.

Day J. M. D., Brandon A. D. and Walker R. J. (2016b) Highly siderophile elements in Earth, Mars, the Moon, and Asteroids. *Rev. Mineral. Geochem.* **81**, 161–238.

Day J. M. D. (2016) Extraordinary world. *Nature* **537**, 310–311.

Day J. M. D., Corder C. A., Cartigny P., Steele A., Assayag N., Rumble, III, D. and Taylor L. A. (2017a) A carbon-rich region in Miller Range 091004 and implications for ureilite Petrogenesis. *Geochim. Cosmochim. Acta* **198**, 379–395.

Day J. M. D., Walker R. J. and Warren J. M. (2017b) ^{186}Os-^{187}Os and highly siderophile element abundance systematics of the mantle revealed by abyssal peridotites and Os-rich alloys. *Geochim. Cosmochim. Acta* **200**, 232–254.

Dhaliwal J. K., Day J. M. D., Corder C. A., Tait K. T., Marti K., Assayag N., Cartigny P., Rumble, III, D. and Taylor L. A. (2017) Early metal-silicate differentiation during planetesimal formation revealed by acapulcoite and lodranite meteorites. *Geochim. Cosmochim. Acta* **216**, 115–140.

Day J. M. D., Tait K. T., Udry A., Moynier F., Liu Y. and Neal C. R. (2018) Martian magmatism from plume metasomatized mantle. *Nat. Commun.* **9**(1), 4799.

Dunaway J.K., Moersch J. and Taylor L.A. (2006) Petrogenesis and potential pairing of the Kunashak and Park Forest chondrites. *Lunar and Planet. Sci.*, *XXXVII*. Lunar Planet. Inst., Houston. #1891 (absr.).

Dunn T. L., Gross J., Ivanova M. A., Runyon S. E. and Bruck A. M. (2016) Magnetite in the unequilibrated CK chondrites: Implications for Metamorphism and new insights into the relationship between the CV and CK chondrites. *Meteorit. Planet. Sci.* **51**, 1701–1720.

Fischer-Gödde M., Becker H. and Wombacher F. (2010) Rhodium, gold and other highly siderophile element abundances in chondritic meteorites. *Geochim. Cosmochim. Acta* **74**, 356–379.

Fischer-Gödde M., Elfers B.-M., Müker C., Szilas K., Maier W. D., Messling N., Morishita T., Kranendonk M. V. and Smithies H. (2020) Ruthenium isotope vestige of Earth's pre-late-veneer mantel preserved in Archaean rocks. *Nature* **579**, 240–244.

Fischer-Gödde M. and Becker H. (2012) Osmium isotope and highly siderophile element constraints on ages and nature of meteoritic components in ancient lunar impact rocks. *Geochim. Cosmochim. Acta* **77**, 135–156.

Fischer-Gödde M. and Kleine T. (2017) Ruthenium isotopic evidence for an inner Solar System origin of the late veneer. *Nature* **541**, 525–527.

Friedrich J. M., Wang M.-S. and Lipschutz M. E. (2002) Comparison of the trace element composition of Tagish Lake with other primitive carbonaceous chondrites. *Meteorit. Planet. Sci.* **37**, 677–686.

Geiger T. and Bischoff A. (1989) (Os, Ru, Ir)S_2 and other refractory siderophile element-rich particles in the metamorphosed carbonaceous chondrites Karoonda, Mulga (West) and PCA82500. *Lunar and Planet. Sci., XX*. Lunar Planet. Inst., Houston, 335–336.

Goderis S., Brandon A. D., Mayer B. and Humayun (2017) Osmium isotopic homogeneity in the CK carbonaceous chondrites. *Geochim. Cosmochim. Acta* **216**, 8–27.

Gopalan K. and Wetherill G. W. (1970) Rubidium-Strontium studies on enstatite chondrites: Whole meteorite and mineral isochrons. *J. Geophys. Res.* **74**, 3457–3467.

Greshake A. (2014) A strongly hydrated microclast in the Rumuruti chondrite NWA 6828: Implications for the distribution of hydrous material in the solar system. *Met. Planet. Sci.* **49**, 824–841.

Heck P. R., Greer J., Boesenberg J. S., Bouvier A., Caffee M. W. and Cassata W. S., et al. (2020) The fall, recovery, classification, and initial characterization of the Hamburg, Michigan H4 chondrite. *Met. Planet. Sci.* **55**(11), 2341–2359.

Hopp T. and Kleine T. (2018) Nature of late accretion to Earth inferred from mass-dependent Ru isotopic composition of chondrites and mantle peridotites. *Earth Planet. Sci. Lett.* **494**, 50–59.

Horan M. F., Walker R. J., Morgan J. M., Grossman J. N. and Rubin A. E. (2003) Highly Siderophile elements in chondrites. *Chem. Geol.* **196**, 5–20.

Huber H., Rubin A. E., Kallemeyn G. W. and Wasson J. T. (2006) Siderophile-element anomalies in CK carbonaceous chondrites: Implications for parent-body aqueous alteration and terrestrial weathering of sulfides. *Geochim. Cosmochim. Acta* **70**, 4019–4037.

Hyde B. C., Day J. M. D., Tait K. T., Ash R. D., Holdsworth D. W. and Moser D. E. (2014) Characterization of weathering and heterogeneous mineral phase distribution in brachinite Northwest Africa 4872. *Meteorit. Planet. Sci.* **49**, 1141–1156.

Jarosewich E., Clarke R. S. and Barrows J. N. (1987) The Allende meteorite reference sample. *Smithson. Contrib. Earth Sci.* **27**, 1–49.

Javoy M., Kaminski E., Guyot F., Andrault D., Sanloup C., Moreira M., Labrosse S., Jambon A., Agrinier P., Davaille A. and Jaupart C. (2010) The chemical composition of the Earth: Enstatite chondrite models. *Earth Planet. Sci. Lett.* **293**, 259–268.

Jochum K. P. (1996) Rhodium and other platinum-group elements in carbonaceous chondrites. *Geochim. Cosmochim Acta* **60**(17), 3353–3357.

Jochum K. P., Nohl U., Herwig K., Lammel E., Stoll B. and Hofmann A. W. (2005) GeoReM: a new geochemical database for reference materials and isotopic standards. *Geostand. Geoanal. Res.* **29**, 333–338.

Kadlag Y. and Becker H. (2015) Fractionation of highly siderophile and chalcogen elements in components of EH3 chondrites. *Geochim. Cosmochim. Acta* **161**, 166–187.

Kadlag Y. and Becker H. (2017) Origin of highly siderophile and chalcogen element fractions in the components of unequilibrated H and LL chondrites. *Geochem.* **77**, 105–119.

Kallemeyn G. W. and Wasson J. T. (1981) The compositional classification of chondrites-I. The carbonaceous chondrite groups. *Geochim. Cosmochim. Acta* **45**, 1217–1230.

Kallemeyn G. W., Rubin A. E., Wang D. and Wasson J. T. (1989) Ordinary chondrites: bulk compositions, classification, lithophile-element fractionation, and composition petrographic type relationships. *Geochim. Cosmochim. Acta* **53**, 2747–2767.

Kallemeyn G. W. and Wasson J. T. (1986) Composition of enstatite (EH3, EH4,5 and EL6) chondrites: implications regarding their formation. *Geochim. Cosmochim. Acta* **50**, 2153–2164.

Kallemeyn G. W., Rubin A. E. and Wasson J. T. (1991) The compositional classification of chondrites: V. The Karoonda (CK) group of carbonaceous chondrites. *Geochim. Cosmochim. Acta* **55**, 881–892.

Kaushal S. K. and Wetherill G. W. (1970) Rubidium 87-Strontium 87 Age of Carbonaceous Chondrites. *J. Geophys. Res.* **75**, 463–468.

Keller L. P., Clark J. C., Lewis C. F. and Moore C. B. (1992) Maralinga, a metamorphosed carbonaceous chondrite found in Australia. *Meteoritics* **27**, 87–91.

Kimura K., Lewis R. S. and Anders E. (1974) Distribution of gold and rhenium between nickel-iron and silicate melts: implications for the abundance of siderophile elements on the Earth and Moon. *Geochim. Cosmochim. Acta* **38**, 683–701.

Krot A. N., Petaev M. I., Scott E. R. D., Choi B.-G., Zolensky M. E. and Keil K. (1998) Progressive alteration in CV3 chondrites: More evidence of astrodial alteration. *Meteorit. Planet. Sci.* **33**, 1065–1085.

Krot A. N., Keil K., Goodrich C. A., Weisberg M. K. and Scott E. R. D. (2004) Classification of meteorites. In *Treatise of Geochemistry* (ed. A. M. Davis). Elsevier-Pergamon, pp. 83–128.

Kruijer T. S., Burkhardt C., Budde G. and Kleine T. (2017) Age of Jupiter inferred from the distinct genetics and formation times of meteorites. *Proc. Nat. Acad. Sci.* **114**, 6712–6716.

Lauretta, D.S., McSween, H.Y. eds. (2006) Meteorites and the Early Solar System II. University of Arizona Press.

Lee M. R. and Bland P. A. (2004) Mechanisms of weathering of meteorites recovered from hot and cold deserts and the formation of phylosilicates. *Geochim. Cosmochim. Acta* **68**, 893–916.

Mann U., Frost D. J., Rubie D. C., Becker H. and Audétat A. (2012) Partitioning of Ru, Rh, Pd, Re, Ir and Pt between liquid metal and silicate at high pressures and high temperatures – implications for the origin of highly siderophile element concentrations in the Earth's mantle. *Geochim. Cosmochim. Acta* **84**, 593–613.

Marty B. (2012) The origins and concentrations of water, carbon, nitrogen and noble gases on Earth. *Earth Planet. Sci. Lett.* **313–314**, 56–66.

McDonald I., Andreoli M. A. G., Hart R. J. and Tredoux M. (2001) Platinum group elements in the Morokweg impact structure, South Africa: evidence for the impact of a large ordinary chondrite projectile at the Jurassic-Cretaceous boundary. *Geochim. Cosmochim. Acta* **65**, 299–309.

McDonough W. F. and Sun S. (1995) The composition of the Earth. *Chem. Geol.* **120**, 223–253.

McIntosh E. C., Day J. M. D., Liu Y. and Jiskoot C. (2020) Examining the compositions of impactors striking the Moon using Apollo impact melt coats and anorthositic regolith breccia meteorites. *Geochim. Cosmochim. Acta* **274**, 192–210.

Meisel T., Walker R. and Morgan J. (1996) The osmium isotopic composition of the Earth's primitive upper mantle. *Nature* **383**, 517–520.

Minster J.-F., Ricard L.-P. and Allègre C. J. (1979) ^{87}Rb-^{87}Sr chronology of enstatite meteorites. *Earth Planet. Sci. Lett.* **44**, 420–440.

Minster J.-F. and Allègre C. J. (1979a) ^{87}Rb-^{87}Sr chronology of H chondrites: Constraint and speculations on the early evolution of their parent body. *Earth Planet. Sci. Lett.* **42**, 333–347.

Minster J.-F. and Allègre C. J. (1979b) ^{87}Rb-^{87}Sr dating of L chondrites: effects of shock and brecciation. *Meteoritics* **14**, 235–248.

Minster J.-F. and Allègre C. J. (1981) ^{87}Rb-^{87}Sr dating of LL chondrites. *Earth Planet. Sci. Lett.* **56**, 89–106.

Minster J.-F., Birck J.-L. and Allègre C. J. (1982) Absolute age of formation of chondrites studied by the ^{87}Rb-^{87}Sr method. *Nature* **300**, 414–419.

Mittlefehldt D. W. and Wetherill G. W. (1979) Rb-Sr studies of CI and CM chondrites. *Geochim. Cosmochim. Acta* **43**, 201–206.

Morgan J. W., Janssens M.-J., Takahashi H., Hertogen J. and Anders E. (1985) H-chondrites: trace element clues to their origin. *Geochim. Cosmochim. Acta* **49**, 247–259.

Murthy V. R. and Compston W. (1965) Rb-Sr ages of chondrules and carbonaceous chondrites. *J. Geophys. Res.* **70**, 5297–5307.

Narayan C. and Goldstein J. I. (1985) A major revision of the iron meteorite cooling rates-An experimental study of the growth of the Widmanstätten pattern. *Geochim. Cosmochim. Acta* **49**, 397–410.

Noguchi T. (1993) Petrology and mineralogy of the CK chondrites: Implications for the metamorphism of the CK chondrite parent body. *Proc. NIPR Symp. Antarct. Meteor.* **7**, 30–41.

Norman M. D. and Mittlefehldt D. W. (2001) Impact processing of chondritic planetesimals: Siderophile and volatile element fractionation in the Chico L chondrite. *Meteorit. Planet. Sci.* **37**, 329–344.

Özdemir S., Schulz T., van Acken D., Luguet A., Reimold W. U. and Koeberl C. (2019) Meteoritic highly siderophile element and Re-Os isotope signatures of Archean spherule layers from the CT3 drill core, Barberton Greenstone Belt, South Africa. *Meteorit. Planet. Sci.* **10**, 2203–2216.

Palme H. and Wlotzka F. (1976) A metal particle from a Ca,Al-rich inclusion from the meteorite Allende, and the condensation of refractory siderophile elements. *Earth Plant. Sci. Lett.* **33**, 45–60.

Peslier A. H. (2020) The origins of water. *Science* **369**(6507), 1058.

Puchtel I. S., Walker R. J., James O. B. and Kring D. A. (2008) Osmium isotope and highly siderophile element systematics of lunar impact melt breccias: Implications for the late accretion history of the Moon and Earth. *Geochim. Cosmochim. Acta* **72**, 3022–3042.

Rankenburg K., Brandon A. D. and Humayun M. (2007) Osmium isotope systematics of ureilites. *Geochim. Cosmochim. Acta* **71**, 2402–2413.

Righter K., Abell P., Agresti D., Berger E. L., Burton A. S., Delaney J. S., Fries M. D., Gibson E. K., Haba M. K., Harrington R., Herzog G. F., Keller L. P., Locke D., Lindsay F. N., McCoy T. J., Morris R. V., Nagao K., Nakamura-Messenger K., Niles P. B., Nyquist L. E., Park J., Peng Z. X., Shih C.-Y., Simon J. I., Swisher C. C., Tappa M. J., Turrin B. D. and Zeigler R. A. (2015) Mineralogy, petrology, chronology, and exposure history of the Chelyabinsk meteorite and parent body. *Meteorit. Planet. Sci.* **50**, 1790–1819.

Righter K. and Drake M. J. (1997) Metal-silicate equilibrium in a homogeneously accreting earth: new results for Re. *Earth Planet. Sci. Lett.* **146**, 541–553.

Roy-Barman M. (1993) Mesure du rapport^{187}Os/^{186}Os dans les basaltes et le péridotites: Contribution de la systématique^{187}Re-^{187}Os dans le manteau. *Ph.D. thesis, Univ. Paris.*

Rubin A. E. (1990) Kamacite and olivine in ordinary chondrites: Intergroup and intragroup relationships. *Geochim. Cosmochim. Acta* **54**, 1217–1232.

Rubin A. E., Huber H. and Wasson J. T. (2009) Possible impact induced refractory-lithophile fractionations in EL chondrites. *Geochim. Cosmochim. Acta* **73**, 1523–1537.

Rubin A. E. (2013) Secrets of primitive meteorites. *Sci. Am.*, 37–41, February 2013.

Rumble D., Farquhar J., Young E. D. and Christensen C. P. (1997) In situ oxygen isotope analysis with an excimer laser using F_2 and Br F_5 reagents and O_2 gas as analyte. *Geochim. Cosmochim. Acta* **61**, 4229–4234.

Schmitz B., Yin Q.-Z., Sanborn M. E., Tassinari M., Caplam C. E. and Huss G. R. (2016) A new type of solar-system material recovered from Ordovician marine limestone. *Nat. Commun.* **7**, 1–7.

Smoliar M. I., Walker R. J. and Morgan J. W. (1996) Re-Os ages of group IIA, IIIA, IVA, and IVB iron meteorites. *Science* **271**, 1099–1102.

Stracke A., Palme H., Gellissen M., Münker C., Kleine T., Birbaum K., Günther D., Bourdon B. and Zipfel J. (2012) Refractory element fractionation in the Allende meteorite: Implications for solar nebula condensation and the chondritic composition of planetary bodies. *Geochim. Cosmochim. Acta* **85**, 114–141.

Swindle T. D., Kring D. A., Burkland M. K., Hill D. H. and Boynton W. V. (1998) Noble gases, bulk chemistry, and petrography of olivine-rich achondrites Eagles Nest and Lewis Cliff 88763: Comparison to brachinites. *Met. Planet. Sci.* **33**, 31–48.

Sylvester P. J., Ward B. J., Grossman L. and Hutcheon I. D. (1990) Chemical compositions of siderophile element-rich opaque assemblages in an Allende inclusion. *Geochim. Cosmochim. Acta* **54**, 3491–3508.

Sylvester P. J., Simon S. B. and Grossman L. (1993) Refractory inclusions from the Leoville, Efremovka, and Vigarano C3V chondrites: major element differences between types A and B, and extraordinary refractory siderophile element compositions. *Geochim. Cosmochim. Acta* **57**, 3763–3784.

Tagle R. and Berlin J. (2008) A database of chondrite analyses including platinum group elements, Ni, Co, Au, and Cr: Implications for the identification of chondritic projectiles. *Met. Planet. Sci.* **43**, 541–559.

Tait K. T. and Day J. M. D. (2018) Chondritic late accretion to Mars and the nature of shergottite reservoirs. *Earth Planet. Sci. Lett.* **494**, 99–108.

Takahashi H., Janssens M-, Morgan J. W. and Anders E. (1978) Further studies of trace elements in C3 chondrites. *Geochim. Cosmochim. Acta* **42**, 97–106.

van Acken D., Brandon A. D. and Humayun M. (2011) High-precision osmium isotopes in enstatite and Rumuruti chondrites. *Geochim. Cosmochim. Acta* **75**, 4020–4036.

Warren P. (2011) Stable-isotopic anomalies and the accretionary assemblage of the Earth and Mars: A subordinate role for carbonaceous chondrites. *Earth Planet. Sci. Lett.* **311**, 93–100.

Walker R. J., Horan M. F., Morgan J. W., Becker H., Grossman J. N. and Rubin A. E. (2002) Comparative Re-Os systematics of chondrites: Implications regarding early Solar System processes. *Geochim. Cosmochim. Acta* **66**, 4187–4201.

Walker R. J., Yin Q.-Z. and Heck P. R. (2018) Rapid effects of terrestrial alteration on highly siderophile elements in the Sutter's Mill meteorite. *Meteorit. Planet. Sci.* **53**, 1500–1506.

Wang Z. and Becker H. (2013) Ratios of S, Se and Te in the silicate Earth require a volatile-rich late veneer. *Nature* **499**, 328–331.

Yokoyama T. and Walker R. J. (2016) Nucleosynthetic isotope variations of siderophile and chalcophile elements in the solar system. *Rev. Mineral. Geochem.* **81**, 107–160.

Yurimoto H., Krot A. N., Choi B-, Aléon J., Kunihiro T. and Brearley A. J. (2008) Oxygen isotopes of chondritic components. *Rev. Min. Geochem.* **68**, 141–186.

Associate editor: Alexander N. Krot